~~River floods in the Anthropocene impact sea-floor geochemistry, pollutants and bacterial communities in coastal systems~~the Adriatic River flooding drives sediment and contaminant redistribution and shapes benthic microbial communities in a Mediterranean coastal system

Claudio Pellegrini[1], Marco Basili[2], Irene Sammartino[1]*, Tommaso Tesi[3], Emanuela Frapiccini[2], Grazia Marina Quero[2-4], Sarah Pizzini[2-5], Roberta Zangrando[3], Gianmarco Luna[2-4], Sara Catena[1], Bruno Campo[6], Naomi Massaccesi[2-4-6], Fabio Trincardi[7], Andrea Gallerani[1], Jacopo Chiggiato[1].

[1]*Consiglio Nazionale delle Ricerche, Istituto di Scienze Marine (CNR-ISMAR), Italy*
[2] *Consiglio Nazionale delle Ricerche, Istituto per le Risorse Biologiche e le Biotecnologie Marine (CNR-IRBIM), Italy*
[3] *Consiglio Nazionale delle Ricerche, Istituto di Scienze Polari (CNR-ISP), Italy*
[4] *NBFC, Centro Nazionale per la Biodiversità, Palermo, 90133, Italy*
[5] *FMC, Fano Marine Center, Italy*
[6] *Alma Mater Studiorum — Università di Bologna, Italy*
[7] *Seas Geosciences (Sealaska) Roma, Italy*

Correspondence to: Irene Sammartino (irene.sammartino@cnr.it)

Abstract. This study examines the sedimentary and microbial responses offshore the Marche Region (Italy) to the September 2022 flood, one of the most severe recent hydrological events, which delivered large amounts of sediment and anthropogenic contaminants to the Adriatic Sea. We employed a multidisciplinary approach integrating sedimentology, geochemistry, organic matter analysis, pollutant assessments (Polycyclic Aromatic Hydrocarbons, PAHs and Poly- and Perfluorinated alkyl substances, PFASs), and benthic microbial community structure. Sediments collected five days after the event offshore river mouths reveal that flood deposits, ranging from fine sand to coarse silt, were largely confined to the nearshore zone, whereas finer clay particles were dispersed offshore down to the 15 m isobath.~~Sediments collected five days post-event offshore six river mouths reveal that flood deposits, ranging from fine sand to coarse silt, were largely confined within the nearshore zone down to the 15 m isobath.~~ This distribution reflects intense riverine inputs and a brief windstorm-enhanced coastal circulation that generated patchy, temporary sediment accumulations mainly in the prodelta sector. Simultaneously, the flood introduced strong spatial heterogeneity in benthic bacterial communities, with sediment texture and organic matter content driving compositional shifts. Freshwater-associated taxa became prominent in prodelta deposits, highlighting riverine sedimentary

imprints. Heavy metal concentrations remained below regulatory thresholds, whereas organic pollutants were heterogeneously distributed, with peaks offshore urban and industrial zones. PAH signatures indicate mixed pyrogenic and petrogenic sources, while next-generation PFASs (6:2FTS) showed localized but severe contamination linked to upstream industrial activities. ~~Simultaneously, the flood introduced strong spatial heterogeneity in benthic bacterial communities, with sediment texture and organic matter content driving compositional shifts. Freshwater-associated taxa became prominent in offshore deposits, highlighting riverine sedimentary imprints.~~ Despite the flood's magnitude onshore, its offshore sedimentary ~~and ecological~~ signatures ~~were~~resulted ephemeral and spatially limited ~~and ephemeral~~. These findings underscore the ecological significance of episodic sediment and contaminant inputs, while highlighting the challenges in detecting such transient events in the marine stratigraphic record.

1. INTRODUCTION

Climate warming is intensifying precipitation extremes globally, with record-breaking daily rainfall events increasing since the 1980s (Allan and Soden, 2008; Westra et al., 2013; Lehmann et al., 2015; Nie et al., 2018; Merz et al., 2021; Sun et al., 2021; Fowler et al., 2021; IPCC, 2023). These changes drive shifts in river discharge patterns and exacerbate flood hazards worldwide, which are expected to worsen due to urbanization, soil degradation, and expanding flood-prone areas (Kundzewicz et al., 2014; Blöschl et al., 2017; Do et al., 2017; Semenza et al., 2020; Slater et al., 2021; Syvitski et al., 2022; Dottori et al., 2023). Extreme river floods abruptly alter coastal ecosystems by delivering freshwater (Vörösmarty et al., 2003), sediments (Rozemeijer et al., 2021; Xin et al., 2023), nutrients (Gao et al., 2018; Lin et al., 2022), organic matter (Bao et al., 2016; Bianchi et al., 2018), pollutants (Weiss et al., 2024; Adeoba et al., 2025) and microbes (Chen et al., 2018), that reshape salinity, sediment regimes, and biogeochemical conditions (Rillig et al., 2015; Lin et al., 2022; Yao et al., 2024). Floods promote microbial dispersal and community shifts, impacting carbon cycling, redox processes, and contaminant dynamics (Reed and Martiny, 2013; Jia et al., 2017; Nakatsu et al., 2019; Yan et al., 2019; Yao et al., 2024; Lin et al., 2022; Zhang et al., 2022; Jia et al., 2017; DesRosiers et al., 2022 Gao and Guo, 2022; Zhang et al., 2022, 2023; Li et al., 2024; Ning et al., 2024). However, how sedimentological controls such as grain-size-dependent transport modulate these biological responses during floods is still not well constrained.

In this scenario, small- to moderate-sized rivers (10^2–10^5 km^2), which are far more numerous than large rivers discharging into coastal zones, play a key role in sediment dynamics on continental shelves (Syvitski and Kettner, 2007; Pitarch et al., 2019).

Flood events in these rivers typically coincide with stormy marine conditions, influencing the preservation and spatial distribution of flood deposits offshore (Syvitski and Kettner, 2007; Wheatcroft et al., 2006; Pellegrini et al., 2021, 2024). Suspended sediment concentrations in such rivers increase non-linearly with discharge, making short-lived flood events the dominant mechanism of sediment delivery to coastal systems (Milliman and Syvitski, 1992; Syvitski et al., 2003; Cohen et al., 2022; Pierdomenico et al., 2022). In fact, most of the sediment flux from small rivers likely occurs during short-lived (days to weeks) flood events (e.g., Blöschl, 2000; Wheatcroft and Drake, 2003; Winsemius et al., 2016; Merz et al., 2021), highlighting the critical role of floods in coastal sedimentation. Studying these flood deposits requires rapid event-response sampling, often challenging due to unpredictability and logistic constraints, especially in dynamic shallow-water environments like deltas where pollutant and microbial community distributions are critical but hard to access immediately post-flood (Wheatcroft, 2000; Trincardi et al., 2020; Pellegrini et al., 2023).

In recent decades, significant efforts have been made to understand the key depositional processes shaping subaqueous coastal environments (e.g. Goodbred et al., 2003; Liu et al., 2006; Korus and Fielding, 2015; Vona et al., 2025). Sedimentary structures formed during floods reflect complex interactions of sediment supply, hydrodynamics, and biological processes, providing essential insights into depositional conditions and coastal sediment dynamics (Nittrouer et al., 1986; Bentley & Nittrouer, 2003; Bhattacharya and MacEachern, 2009; Jaramillo et al., 2009; Macquaker et al., 2010; Ainsworth et al., 2011; Peng et al, 2022; Pellegrini et al., 2024). Marine sediments also act as reactive interfaces and sinks for contaminants, influencing marine food webs through episodic resuspension and bioaccumulation (Roberts, 2012). Benthic microbial communities at the sediment-water interface mediate organic matter degradation, nutrient cycling, and contaminant transformation, yet their spatial organization and responses to flood-driven sediment heterogeneity remain poorly understood (Voynova et al., 2017; Danovaro et al., 2012; Trouche et al., 2021).

Acting as both reactive interfaces and long-term sinks, sediments accumulate contaminants that can be episodically resuspended and bioaccumulated, with cascading effects across marine food webs (Roberts, 2012). Within this dynamic environment, benthic microbial communities occupy the critical boundary between the water column and the subseafloor (Voynova et al., 2017; Liu et al., 2020; Trouche et al., 2021), where they play fundamental roles in organic matter degradation, nutrient cycling, and contaminant transformation (Danovaro et al., 2012; Steichen et al., 2020; Checchi et al., 2021; Jiajun et

al., 2024). Furthermore, hypopycnal coastal plumes foster intense new primary productivity, adding another source of organic biomass accumulating at the seafloor along the shelf (Lohrenz et al., 1990; Campanelli et al., 2011; Vona et al., 2025). Despite their importance, the factors controlling the spatial organization and functioning of these communities remain incompletely understood, particularly in dynamic coastal settings where sediment suspension, deposition, erosion, and alongshore transport interact with pronounced small-scale heterogeneity (Clark et al., 2021; Trouche et al., 2021).

Coastal systems are a temporary storage for river-borne sediments (e.g., Bao et al., 2016; Bianchi et al., 2018; Pellegrini et al., 2021, 2024) and can accumulate anthropogenic materials catchments (Simon-Sánchez et al., 2019; Lim et al., 2021; Pierdomenico et al., 2022; Pellegrini et al., 2023; Trincardi et al., 2023; Bolan et al., 2024; Iemelianov et al., 2024; Weiss et al., 2024; Bue et al., 2025; Gruca-Rokosz et al., 2025; Jalaosho et al., 2025; Nikki et al., 2025; Owowenu et al., 2025), especially in prodeltas, that are the delta sector lying beyond the delta front in a submerged environment where the highest sediment accumulation rate are reached (Coleman and Wright, 1975; Pellegrini et al., 2020). Riverine sediments play a fundamental role in the supply of hazardous metals and other contaminants to coastal areas, often reflecting significant sources of pollution (e.g. Lucchini et al., 2001; Sammartino, 2004; Amorosi and Sammartino, 2007; Jeon et al., 2011; Munoz et al., 2017; Amorosi et al., 2022; Riminucci et al., 2022; Fanelli et al., 2025; Frapiccini et al., 2024). Among coastal environments, river deltas are particularly dynamic, responding rapidly to both natural and anthropogenic changes (Syvitski et al., 2005, 2009; Blum and Roberts, 2009; Overeem and Brakenridge, 2009; Falcini et al., 2012; Anthony et al., 2014; Bosman et al., 2020; Trincardi et al., 2020; Syvitski et al., 2022; Gardner et al., 2023; Haq and Milliman, 2023; Anthony et al., 2024; Warrick et al., 2024; Ohenhen et al., 2026).

This study addresses this gap by studying the September 2022 flood in the Marche region (Fig. 1) as a rare observational opportunity. Samples were strategically collected from freshly deposited surface sediments and from underlying, pre-flood bottom deposits, allowing for a direct comparison to isolate the effects of the flood. By capturing sedimentary, geochemical, and biological signals shortly after the event, we provide novel insights into early deposition processes and spatial patterns triggered by floods. This event-focused approach highlights the added value of timely, targeted sampling in advancing our understanding of pollutant dynamics, microbial responses, and organic carbon fate in transitional environments, ultimately supporting more accurate predictive frameworks and effective mitigation strategies.

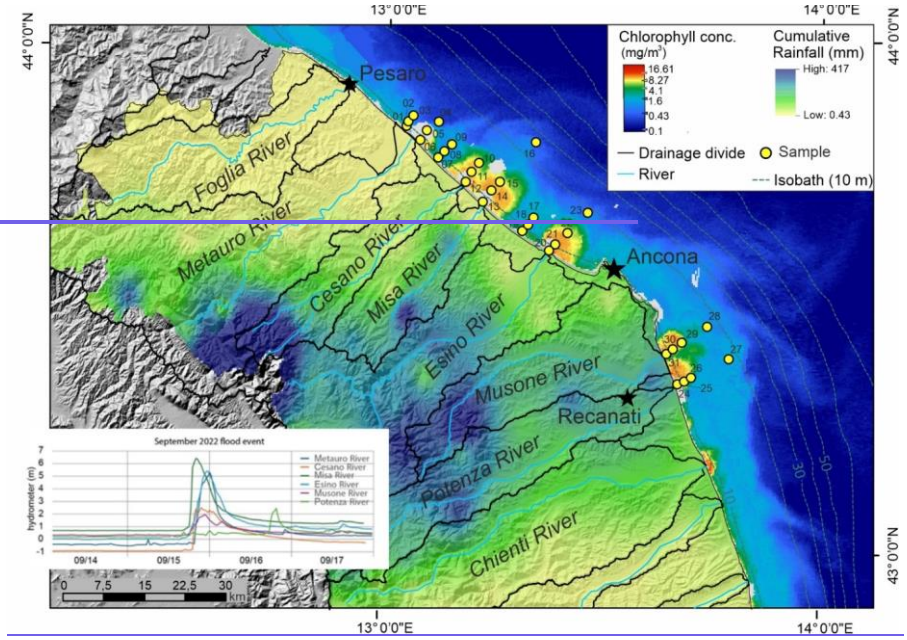
13°0'0"E
14°0'0"E
44°0'0"N
43°0'0"N
Chlorophyll conc. (mg/m³)
16.61
8.27
4.1
1.6
0.43
0.1
Cumulative Rainfall (mm)
High: 417
Low: 0.43
Drainage divide
River
Sample
Isobath (10 m)
Pesaro
Ancona
Recanati
Foglia River
Metauro River
Cesano River
Misa River
Esino River
Musone River
Potenza River
Chienti River
September 2022 flood event
hydrometer (m)
09/14
09/15
09/16
09/17
0 7,5 15 22,5 30 km

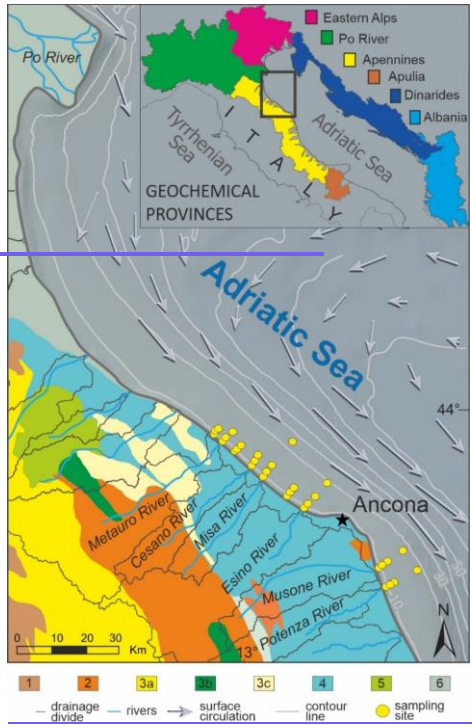
Eastern Alps
Po River
Apennines
Apulia
Dinarides
Albania
Po River
Tyrrhenian Sea
I T A L Y
Adriatic Sea
GEOCHEMICAL PROVINCES
Adriatic Sea
44°
Ancona
Metauro River
Cesano River
Misa River
Esino River
Musone River
Potenza River
13°
0 10 20 30 Km
N
1
2
3a
3b
3c
4
5
6
drainage divide
rivers
surface circulation
contour line
sampling site

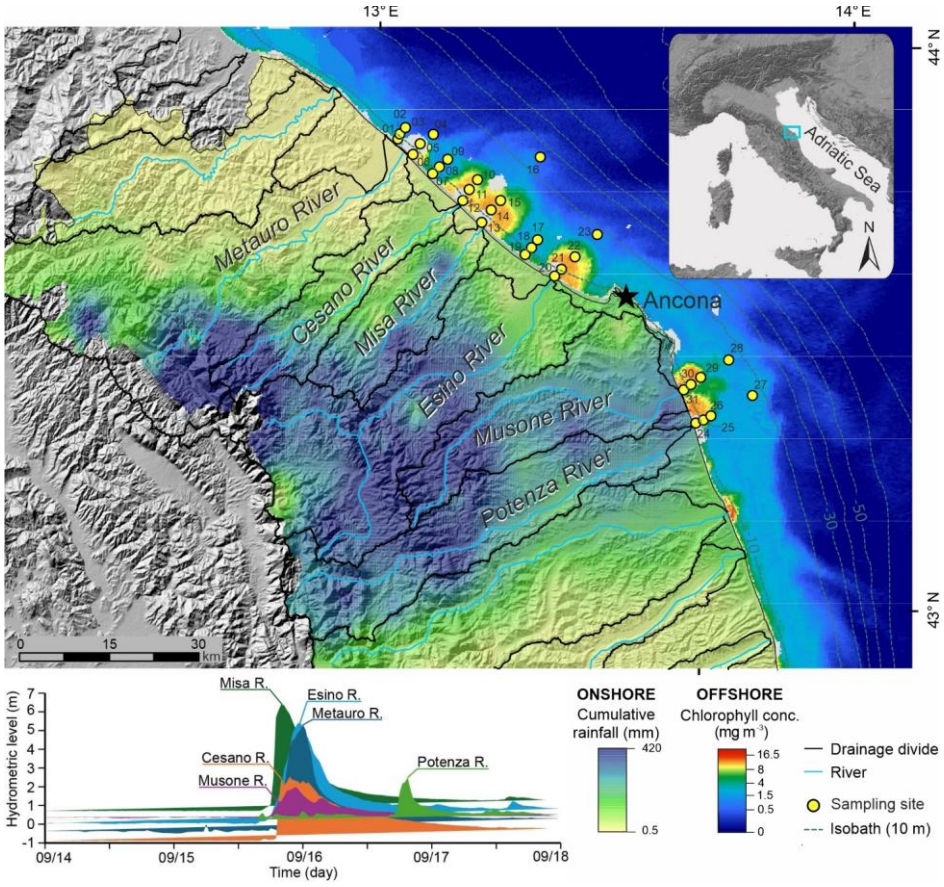

115 **Figure 1:** Study area with cumulative rainfall (in mm) recorded between 4:00 PM on September 15th and 1:00 AM on September 16th, along with river catchments of major rivers affected by the September 2022 flood. Offshore background shading indicates satellite-derived chlorophyll-a concentration (mg m^{-3}) on September 16th as a proxy for surface productivity (from EU Copernicus Marine Service product OCEANCOLOUR_MED_BGC_L3_MY_009_143). Yellow dots show sampling sites at sea.~~Geological and~~

~~hydrographic map of the central Adriatic region, highlighting major river basins in the Marche region (Metauro, Cesano, Misa, Esino, Musone, Potenza). Colors indicate main geological formations; gray lines mark drainage divides. Yellow dots show coastal sampling sites. Gray arrows represent surface circulation (averaged measurements of drifter velocities; Poulain, 2001). Inset: geochemical provinces of northern and central Adriatic Sea as documented in Amorosi et al., 2022, with the study area outlined (black box) and major sediment provenance domains indicated.~~

2. APPROACH

2.1 Study area and the 2022 flood event

On September 17th, a development of a low-pressure system over the central Adriatic Sea led to scattered, thought intense, showers. While hydrodynamics conditions during the flood were quite calm, this low-pressure system rapidly moving across the Adriatic Sea resulted (locally along the coast of the Marche Region) in gale-force northeasterlies during the afternoon (Figs. 2a,b,c), with rapid intensification of the sea state (Fig. 2d) and alongshore (ca. 120°, i.e., toward south-east, see Fig. 2f) currents with peak during the windstorm of 1 m s^{-1} at the surface and 0.7 m s^{-1} near bottom (Fig. 2e). Operational ocean model data (Fig. 2g, h, i) also provide a larger picture of the hydrodynamical response to the windstorm. Although this windstorm was short-lived, associated resuspension and transport alongshore arguably played a role on the fate of the sediment discharged by the flood to the coastal area as discussed in section 5.

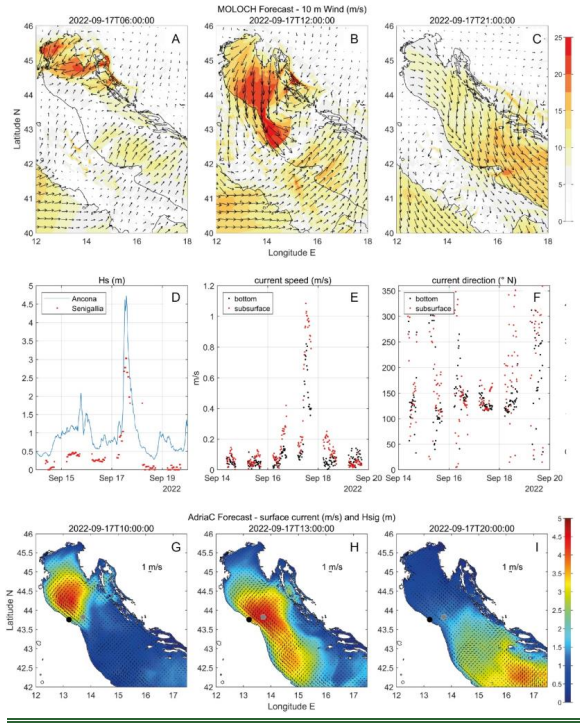

Figure 2~~1~~: 10 m wind (m s^{-1}) MOLOCH forecast valid time 17 September 2022 (A) 06:00 UTC, (B) 12:00 UTC, and (C) 21:00 UTC; (D) significant wave height (m) measured at Ancona (blue line) and Telesenigallia (red dots), (E) ocean currents speed (m s^{-1}) measured by TeleSenigallia ADCP, along with (F) currents direction (degree, 0 N, flowing toward); ADCIRC forecast for significant wave height (m, color coded) and surface currents (black arrows) valid time 17 September (G) 10:00 UTC, (H) 13:00 UTC, (I) 20:00 UTC. The black filled circle indicates TeleSenigallia marine station position. The gray filled circle indicates Ancona wave buoy position. Technical details on the source datasets can be found in the supplementary material.

The September 2022 rainfall event occurred after a prolonged period of drought, that has strongly affected the catchment, and lasted approximatively twelve hours (Donnini et al., 2023; Pulvirenti et al., 2023). On September 15th, several thunderstorms affected the northern and central mountainous and high-hilly areas of the region, with rainfall decreasing in intensity while moving towards the coast. In the late afternoon, a self-regenerating and stationary system formed, eventually affecting also the hills and coastal areas. This system caused widespread critical conditions in the river basins (e.g., Cesano and Misa rivers; De Lucia et al., 2024) with cumulated rain values peaking up to 90 mm/h and 400 mm / 6 h (data from Regione Marche, Centro Funzionale Regionale). As a consequence, river levels rose rapidly~~–~~, by up to five meters in just three hours (Fig. ~~2~~1)~~–~~, with flood thresholds exceeded at multiple sites and widespread inundation reported. On the following day, a similar, yet weaker, thunderstorm system developed to the windward side of the Apennines, affecting additional catchments to the south (i.e., Potenza River, see Fig. ~~2~~1) with cumulated rain peaking up to 140 mm over the event. ~~Finally, a development of a low-pressure system over the central Adriatic Sea on September 17th led to additional scattered showers and to a rapid intensification of winds from the north-east. While hydrodynamics conditions during the flood were quite calm, this low-pressure system rapidly moving across the Adriatic Sea resulted (locally along the coast of the Marche Region) in gale-force northeasterlies during the afternoon (Figure 11a,b,c), with rapid intensification of the sea state (Fig. 11d) and alongshore (ca. 120°, i.e., toward south-east, see Fig. 11f) currents with peak during the windstorm of 1 m s^{-1} at the surface and 0.7 m s^{-1} near bottom (Fig. 11e). Operational ocean model data (Fig. 11g, h, i) also provide a larger picture of the hydrodynamical response to the windstorm. Although this low-pressure system exited this windstorm was short-lived the region by the end of the day, the associated resuspension and transport alongshore arguably played a role windstorm was influential on the fate of the sediment discharged by the flood to the coastal area as discussed in section 5.~~

2.2 The 2022 Rapid Response Cruise (RRC)

~~Surface~~ Sediment samples were collected on board the R/V *Tecnopesca II* on September 23rd, 2022, just five days after the major flooding event that impacted the central Adriatic coast. Sampling took place along nine coast-to-offshore transects, corresponding to six primary river mouths affected by the flood, as well as three intermediate transects (Fig. 1). The number of sampling stations extended offshore until flood-related deposits were no longer detectable. Sediment was retrieved from each station using a 25 L Van Veen grab, which allowed the recovery of approximately 60 kg (25,000 cm^3 x 2.5 g cm^{-3}) of sediment. The flood event produced a distinctive sedimentary deposit, identifiable by its fabric characteristics (i.e. grain size

Formattato: Interlinea: 1,5 righe

and shape, colour, organic matter and water content, sedimentary structures; Lazar et al., 2015) relative to the underlying sediments (Lazar et al., 2015). The grab allowed for the sub-sampling of the sediment succession up to 25 cm in depth to examine the sedimentary expression of the 2022 flood event (Fig. 23).

All sub-samples were labeled with the cruise acronym (Rapid Response Cruise, RRC) and stored in sterilized glass vials. Pollutants analyses were carried out on a subset of sediment samples. Specifically, two sampling points for each of the nine analyzed transects were selected: the first one is located closer to the coast, the second one at the furthest point. For each of these 18 sampling points, two aliquots of sediment were taken: the first one (top) corresponding to the 2022 river flood deposits, the second one (bottom) referring to pre-flood sedimentary deposits. All the analyses are summarized see in the Supplemental Material.

ha formattato: Colore carattere: Azzurro

Formattato: Interlinea: doppia

Formattato: Interlinea: 1,5 righe

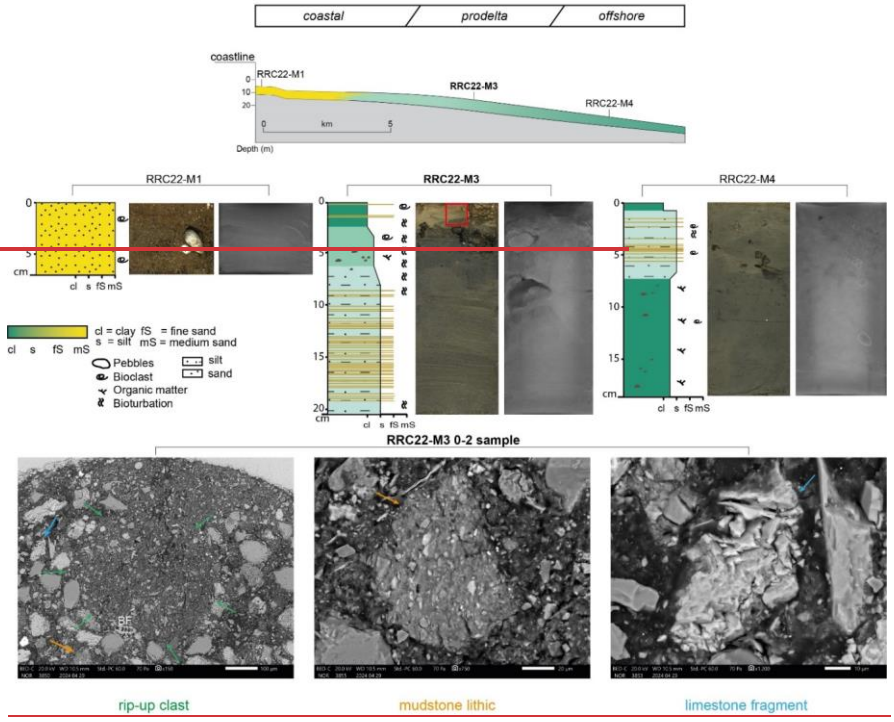
coastal
prodelta
offshore
coastline
RRC22-M1
RRC22-M3
RRC22-M4
0
10
20
0
km
5
Depth (m)
RRC22-M1
RRC22-M3
RRC22-M4
cm
cl s fS mS
cl = clay fS = fine sand
s = silt mS = medium sand
Pebbles
Bioclast
Organic matter
Bioturbation
silt
sand
RRC22-M3 0-2 sample
rip-up clast
mudstone lithic
limestone fragment

185

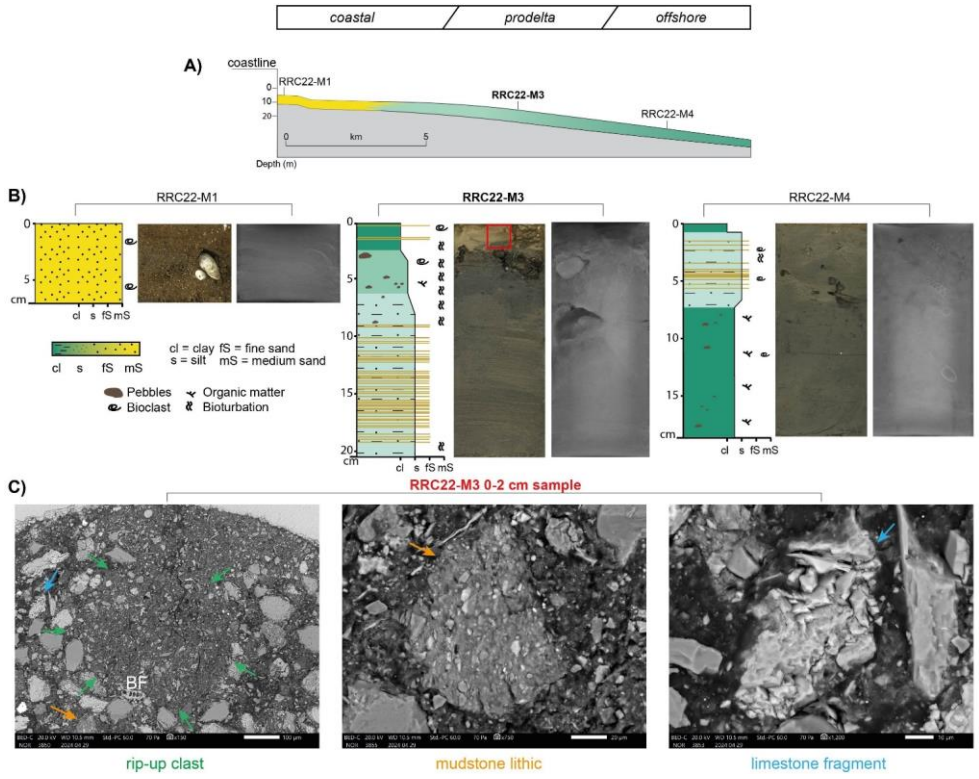

Figure 3: The sedimentary expression of the 2022 river flood along a coast-to-sea transect offshore from the Misa River: a) schematic section based on previously published seismic profiles (e.g., Cattaneo et al., 2003; Pellegrini et al., 2021); b) sedimentary logs illustrating the main lithological changes, sedimentary structures, bioclasts, and bioturbation features; and c) Scanning Electron Microscopy (SEM) images of ion-milled samples from sediment cores with fine-grained intraclasts, semi-consolidated rip-up clast (green arrow), mudstone lithic (orange arrow), limestone fragment (light blue arrow), benthic forams (BF).

~~**Figure 2: Cumulative rainfall (in mm) recorded between 4:00 PM on September 15th and 1:00 AM on September 16th, along with hydrometric levels measured at gauging stations located along major rivers affected by the September 2022 flood: Metauro River (Acqualagna), Cesano River (San Michele al Fiume), Misa River (Bettolelle), Esino River (Camponocchio), Musone River (Montepolesco), and Potenza River (San Severino Marche), on September 16th from EU Copernicus Marine Service product OCEANCOLOUR_MED_BGC_L3_MY_009_143 Yellow dots show sampling sites at sea.**~~

Formattato: Allineato al centro

3. DATA AND METHODS

3.1 Sedimentological analyses on organic and inorganic particles

Sedimentological analyses were conducted at multiple scales, from meter to micron-nanometer resolution. Stratigraphic descriptions coupled with high-resolution photographic images allowed characterization of subtle sedimentary structures in fine-grained sediments. Samples with notable texture changes were selected for Scanning Electron Microscopy (SEM) to investigate sediment fabric and sedimentary processes (Fig. 3). SEM analysis was performed on samples stabilized with resin after pore water removal and ion milling, following established protocols (Schimmelmann et al., 2015; Schieber, 2013; see Supplemental Material). SEM surfaces were examined in low vacuum mode without conductive coating, and Energy Dispersive X-ray Spectroscopy (EDS) was used for compositional analysis.

Granulometric analysis and water content determination were conducted on sediment aliquots from each station, for both flood and pre-flood deposits. Grain size was measured using a Malvern Mastersizer 3000 analyzer (0.01–3500 µm), with samples dispersed and ultrasonicated prior to analysis. Grain-size distributions were processed and reported according to the Wentworth scale (Wentworth, 1922; Blott and Pye, 2001; see Supplemental Material).

Organic matter was characterized at bulk and molecular levels. Sedimentary organic carbon was analyzed through stable carbon isotopes ($\delta_{13}C$) using EA-IRMS, following acidification to remove inorganic carbon (Tesi et al., 2007). A compilation of $\delta_{13}C$ data from terrigenous sources along the Adriatic coast was used to define end-members for source apportionment (Tesi et al., 2013; Pellegrini et al., 2021, 2024; see Supplemental Material). ~~Sedimentological analyses were conducted at different resolutions from m to µm-nm scale. The stratigraphiy description, coupled with high-resolution photographic images, was~~

Formattato: Interlinea: doppia

used to characterize subtle sedimentary structures in fine-grained sediments. A subset of samples, exhibiting noticeable changes in texture, was selected for Scanning Electron Microscope (SEM) analysis to identify sediment fabric and reconstruct the main sedimentary processes (Fig. 3). SEM samples were stabilized with Spurr resin after pore water was removed using acetone (Schimmelmann et al., 2015), and then ion-milled (Schieber, 2013). The same methodology was applied to analyze primary sedimentary structures and fabrics in Holocene Adriatic samples (Pellegrini et al., 2021, 2024). The milled sample surfaces were examined without a conductive coating using a FEI Quanta 400 FEG (Field Emission Gun) in low vacuum mode. Energy Dispersive X-ray Spectroscopy (EDS) was used to determine the composition of the sedimentary particles. Granulometric analysis and water content determination were conducted on sediment aliquots from each sampling station for both the 2022 river flood and pre-flood deposits. Approximately one spoonful of wet sediment was weighed using an analytical balance with mass measurements to two decimal places. The sediments were then dried at 50°C for 24 hours, re-weighed, and the ratio of wet to dry sediment mass was calculated. Grain size was determined using a Malvern Mastersizer 3000 analyzer (Hydro EV), which covers size ranges from 0.01 to 3500 µm, at the Geohazard core laboratory of the Institute of Marine Science of the National Research Council (CNR-ISMAR), Bologna. Sediment samples were dispersed in demineralized water for 24 hours and subjected to ultrasonic treatment for 60 seconds prior to analysis. Laser scattering spectra were processed using the Multiple Sample Statistics sheet in the GRADISTAT MS Excel worksheet (Blott and Pye, 2001). The grain-size analysis includes all particles in the sample and results are reported according to the Wentworth scale (Wentworth, 1922). Organic matter characterization was performed at both bulk and molecular levels. Sedimentary organic carbon was analyzed using stable carbon isotopes ($\delta^{13}C$) via EA-IRMS (Elemental Analyzer-Isotope Ratio Mass Spectrometry), following the method outlined by Tesi et al. (2007). In brief, freeze-dried and ground samples were placed in silver capsules, acidified with 1.5 M HCl to remove the inorganic fraction, and analyzed using a Finnigan DeltaQ Mass Spectrometer, directly coupled to a Thermo Fisher Scientific FLASH 2000 IRMS Element Analyzer through a ConFlo IV interface for continuous flow measurements. The standard deviation, based on replicate analyses of the reference standard (IAEA-CH7) and in-house standards, was < ±0.1‰.

$\delta^{13}C$ data from recent studies on the supply and deposition of Terrigenous Organic Carbon (OC_{terr}) along the Adriatic coastal system were compiled to define the terrigenous end-member and provide context for the RRC2022 samples. Our dataset

~~included Po River suspended sediments from the 2011 flood, river bed sediments from the Apennine rivers (2005), and Po River flood deposits (2000-2009). All terrigenous samples displayed the depleted $\delta^{13}C$ signature typical of land-derived material, with an average value of -26.46±0.44‰ (Tesi et al., 2013; Pellegrini et al., 2021, 2024). The marine $\delta^{13}C$ end member (-20.4‰) from Tesi et al. (2006) was used in the source apportionment model.~~

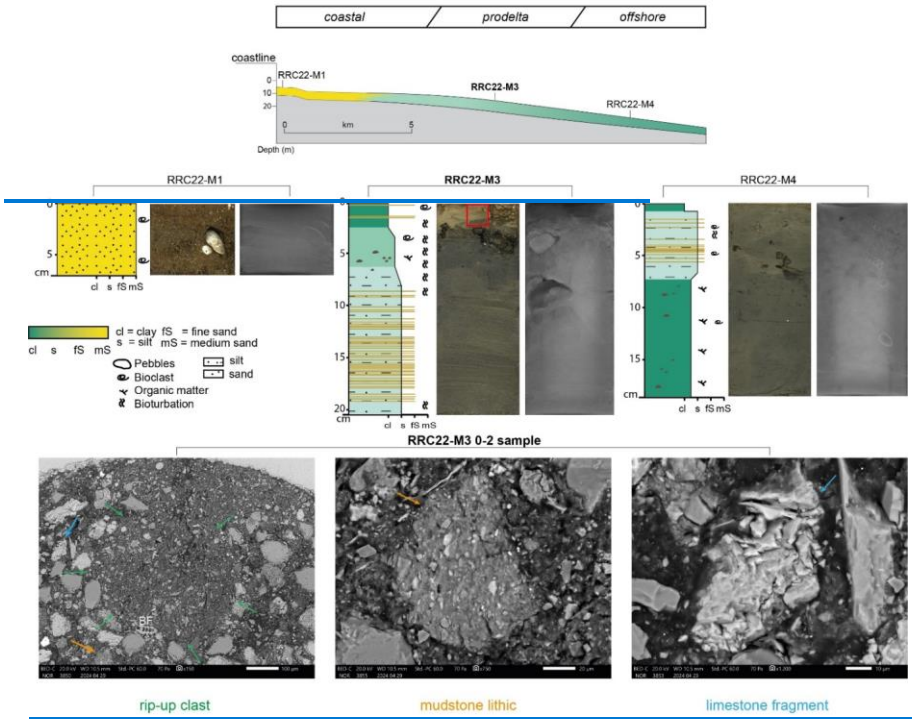

~~**Figure 3: The sedimentary expression of the 2022 river flood along a coast-to-sea transect offshore from the Misa River mouth: a) schematic section based on previously published seismic profiles (e.g., Cattaneo et al., 2003; Pellegrini et al., 2021); b) sedimentary logs illustrating the main lithological changes, sedimentary structures, bioclasts, and bioturbation features; and c) Scanning Electron Microscopy (SEM) images of ion-milled samples from sediment cores**~~

~~with fine-grained intraclasts, semi-consolidated rip-up clast (green arrow), mudstone lithic (orange arrow), limestone fragment (light blue arrow), benthic forams (BF).~~

3.2 X-Ray Fluorescence (XRF)

Geochemical analyses of bulk sediments were conducted using wavelength-dispersive X-ray fluorescence (WD-XRF) to quantify major and trace elements. Forty-two sediment samples were air-dried, ground, and pressed into tablets for analysis at the University of Bologna. Matrix correction methods and accuracy verification via certified reference materials ensured reliable quantification (Govindaraju, 1989; Franzini et al., 1972, 1975; Leoni and Saitta, 1976; Leoni et al., 1986; see Supplemental Material).

Sediment provenance was assessed by comparing geochemical fingerprints to riverine deposits from Alpine and Apennine catchments, which display characteristic elemental signatures reflecting their lithology ~~(Fig. 1)~~ (Dinelli & Lucchini, 1999; Amorosi et al., 2022). Provenance indicators such as Ca-Al_2O_3, Cr-V, and MgO-Ni/Al_2O_3 diagrams were used for interpretation.

~~Geochemical analyses were performed to assess sediment provenance and hazardous metals content. Total concentrations of major and trace elements were determined using Wavelength-Dispersive X-Ray Fluorescence (WD-XRF). A total of 42 bulk sediment samples were analyzed at the University of Bologna. Samples were air-dried at 40°C and ground using an agate swing mill. The powders were then pressed into tablets and analyzed for major and trace elements using a Panalytical Axios spectrometer (Rh tube), applying matrix correction methods by Franzini et al. (1972, 1975), Leoni and Saitta (1976), and Leoni et al. (1986). Accuracy was verified through certified reference materials (Govindaraju, 1989), with uncertainties of 2% for Ni and Zn, 6% for Cu, 7% for Cr, and 10% for As and Pb.~~

~~To reconstruct sediment provenance, data were compared with geochemical analyses of riverine deposits from previous studies. Alpine and Apennine rivers provide distinct geochemical fingerprints reflecting their respective catchment geology (see Amorosi et al., 2022). The Po River basin drains the Western and Central Alps and the Ligurian-Emilian Apennines. The Western Alps are characterized by metamorphic and mafic-ultramafic (ophiolitic) rocks, while the Apennines consist mainly~~

~~of shales, marls, and sandstones, with localized ophiolite exposures. This ultramafic imprint is evident in Po River sediments, which show elevated Cr and Ni concentrations (Fig. 1).~~

~~To assess sediment provenance, Ca-Al_2O_3, Cr-V and MgO-Ni/Al_2O_3 diagrams were used as provenance indicators, plotting major and trace element composition of the study samples against sediment samples from the modern river network (Dinelli & Lucchini, 1999; Amorosi and Sammartino, 2007; Amorosi et al. 2022).~~

3.3 Polycyclic Aromatic Hydrocarbons (PAHs)

Sixteen priority PAHs, including low molecular weight (LMW) and high molecular weight (HMW) compounds, were quantified to assess contamination sources. Extraction was performed using ultrasonic-assisted solvent extraction, followed by UHPLC analysis with diode array and fluorescence detection (Frapiccini et al., 2024). Method validation complied with ICH Q2B guidelines, and recoveries were verified with IAEA reference materials. LODs, LOQs, and recovery rates are reported in Supplemental Tables S1 and S2.

Diagnostic ratios (e.g., LMW/HMW, anthracene/(anthracene + phenanthrene), ΣCOMB/ΣPAHs, fluoranthene/(fluoranthene + pyrene), benz[a]anthracene/(benz[a]anthracene + chrysene)) were calculated to distinguish petrogenic from pyrogenic PAH sources, following literature standards (Yunker et al., 2002; Arienzo et al., 2017; Maletić et al., 2019; Lee et al., 2021; Mali et al., 2022).~~The PAHs analyzed in this study are those listed as priority pollutants by both the European Union and the US EPA. Sixteen compounds were targeted, including low molecular weight (LMW, 2-3 rings) PAHs: naphthalene, acenaphthylene, acenaphthene, fluorene, phenanthrene, and anthracene, and high molecular weight (HMW, ≥4 rings) PAHs: fluoranthene, pyrene, benz[*a*]anthracene, chrysene, benzo[*b*]fluoranthene, benzo[*k*]fluoranthene, benzo[*a*]pyrene, dibenz[*a,h*]anthracene, benzo[*ghi*]perylene, and indeno[1,2,3-*cd*]pyrene. PAHs were extracted using a 50:50 dichloromethane/methanol solution in an ultrasonic bath (BRANSONIC 1510E-mt) for three 15-minute cycles. The extract was concentrated via rotary evaporation at 27°C and under nitrogen flow, then reconstituted in 0.4 mL of acetonitrile. Analyses were conducted via an UHPLC system (UltiMate 3000, Thermo Scientific), equipped with a Diode Array Detector (DAD) and a fluorescence detector (RF2000, Dionex). Instrumental details are reported in Frapiccini et al. (2024). Method validation followed ICH Q2B guidelines (ICH, 2005), using LOD = 3.3 Sa/b and LOQ = 10 Sa/b, where Sa is the standard deviation of the intercept and b is the calibration

~~slope. Recoveries were verified using IAEA-408 and IAEA-383 reference materials. LODs, LOQs, and recovery rates are presented in Tables S1 and S2.~~

~~To investigate PAH sources, diagnostic ratios were used, distinguishing between petrogenic (originating from petroleum) and pyrogenic (from combustion) origins. Ratios calculated include: LMW/HMW, anthracene/(anthracene + phenanthrene), ΣCOMB/ΣPAHs, fluoranthene/(fluoranthene + pyrene), and benz[*a*]anthracene/(benz[*a*]anthracene + chrysene) (Yunker et al., 2002; Arienzo et al., 2017; Maletić et al., 2019). Petrogenic PAHs are typically waterborne and deposited directly in sediments, while pyrogenic PAHs are airborne before entering aquatic systems. ΣCOMB includes fluoranthene, pyrene, benz[*a*]anthracene, chrysene, benzo[*b*]fluoranthene, benzo[*k*]fluoranthene, benzo[*a*]pyrene, indeno[1,2,3-*cd*]pyrene, and benzo[*ghi*]perylene. A ΣCOMB/ΣPAHs ratio > 0.8 indicates a pyrogenic origin; < 0.8 suggests a petrogenic one. Similarly, anthracene/(anthracene + phenanthrene) > 0.1 and fluoranthene/(fluoranthene + pyrene) > 0.5 both point to pyrogenic sources. Conversely, ratios below those thresholds suggest petrogenic origins. Lastly, benz[*a*]anthracene/(benz[*a*]anthracene + chrysene) > 0.35 also implies pyrogenic input (Lee et al., 2021; Mali et al., 2022).~~

3.4 Poly- and Perfluorinated alkyl substances (PFASs)

PFASs were extracted from sediment samples using Accelerated Solvent Extraction (ASE) with methanol under controlled temperature and pressure. Extracts were purified by Solid Phase Extraction and analyzed using HPLC coupled with triple quadrupole LC-MS/MS operated in negative ion mode. Seventeen PFAS analytes, including target and next-generation compounds, were quantified using isotopic dilution with internal standards. The analytical method quality control followed US EPA 1663A guidelines, with repeatability and recovery tests conducted on Pleistocene sediment blanks (Pizzini et al., 2024). Concentrations are reported on a dry weight basis (see Supplemental Table S3).

~~The extraction of the analytes from the matrix was performed using an Accelerated Solvent Extractor (ASE™ 350, Thermo Fisher Scientific Dionex Inc.). About 10 g wet weight of fresh sediment samples were homogenized and mixed with diatomaceous earth (Applied Separations Inc.), anhydrous sodium sulfate, and activated metallic copper (Sigma-Aldrich Co.), to remove humidity and elemental sulfur from samples, then placed in a 20 mL cell and spiked with a known amount of D and ^{13}C isotope-labeled solution. The extractions were carried out at 100 bar and 100°C using~~

~~methanol as extraction solvent. The extraction procedure, 5-minutes static after a 5-min equilibration time, was repeated three times. The extracts were collected together, evaporated at 30°C under a gentle nitrogen stream to 10 mL (Turbovap® II, Caliper Life Science Inc.), and then diluted with 25 mL of deionized water. Clean-up was performed by Solid Phase Extraction (SPE) using Oasis HLB cartridge (Waters Corp.; Hydrophilic-Lipophilic Balance, 500 mg, 6 mL, 60 µm) previously conditioned by passage of 10 mL of methanol, followed by 10 mL of deionized acidified water. The extracts were passed through the cartridges under a pressure of 0.3 bar. The cartridges were then washed with 10 mL of deionized acidified water to remove all the salts and dried by passage of air for 5 min. The analytes were eluted with 10 mL of methanol at a rate of one drop per second and the eluate was diluted 1:1 (v/v) with deionized water. Instrumental analyses were performed using an Agilent 1100 Series HPLC Value System (Agilent Technologies Inc.), coupled with a triple quadrupole API 4000™ LC-MS/MS System, equipped with an ESI Turbo V™ source (Applied Biosystems/MDS SCIEX PTE. Ltd.), operating in negative polarity. Data acquisition was obtained in MRM (Multiple Reaction Monitoring) mode with a 50 ms dwell time/transition. We considered 17 analytes, belonging to both target and next-generation PFASs. Quantification was performed using internal standards and the isotopic dilution technique. Results were corrected using the instrumental response factors and subtracting the procedural blanks. All sediment concentrations were calculated on a dry weight (dw) basis (Tab. S3). The quality control of the entire analytical procedure, in terms of repeatability (expressed as relative standard deviation), trueness (expressed as relative error), and percentage of recovery, was performed on five replicates of a fortified real environmental matrices (sediments collected in the Venice Lagoon at a depth of 10 m, dated back to the Pleistocene age and for these reasons judged free from modern contaminant compounds (Pizzini et al., 2024), and in compliance with the US EPA 1663A method.~~

3.5 Microbial communities

DNA was extracted from the top 0–1 cm sediment layer and amplified targeting the V4–V5 region of the 16S rRNA gene (Parada et al. 2016). Libraries were prepared using the Nextera protocol and sequenced on the Illumina NextSeq2000 platform (2×300 bp). Raw data were processed with Cutadapt for adapter removal, and DADA2 for quality filtering, chimera removal, and ASV inference (Basili et al., 2021; Callahan et al., 2016). Taxonomic classification was performed using SILVA v138.

excluding chloroplast and eukaryotic sequences. Samples with low ASV counts were omitted (see Supplemental Table S2). Abundance normalization and diversity analyses were conducted in R using *vegan* and *phyloseq* packages (Oksanen et al, 2025; McMurdie and Holmes, 2013).

~~DNA was extracted from superficial (uppermost 0-1 cm) sediment samples using the DNeasy PowerSoil Kit (Qiagen) following the protocol described by Basili et al. 2021. Extracted DNA was stored at −20°C until further analysis. Quantification of DNA was followed by PCR amplification targeting the V4–V5 hypervariable region of the 16S rRNA gene using the primer pair 518F-926R. PCR products were purified and indexed libraries prepared using the Nextera library preparation protocol and sequenced on the Illumina NextSeq2000 platform using a 2 × 300 bp paired-end protocol. Raw sequence data were processed using Cutadapt (Martin, 2011) to remove primer and adapter sequences. Paired-end reads were imported and analyzed in RStudio (version 4.4.0) with the DADA2 package (version 1.32) (Callahan BJ, et al. 2016). Quality filtering was performed according to DADA2 guidelines, using maximum allowable estimated errors of >2 and 2 per read for forward and reverse reads, respectively. Reads were merged into amplicon sequence variants (ASVs) based on 100% sequence identity. Chimeric sequences were identified and removed. Taxonomic classification was conducted using a naive Bayesian classifier against the SILVA database (version 138). Chloroplast and eukaryotic sequences were excluded from the dataset, and samples with low ASV counts were omitted (Table S2). Abundance values were normalized using the median of the dataset with the vegan (version 6.1) (Oksanen et al., 2025) and phyloseq (version 1.48) (McMurdie and Holmes, 2013) R packages and subsequently converted to relative abundances for further analyses. Raw sequence files are freely available in the Sequence Read Archive (NCBI SRA, https://www.ncbi.nlm.nih.gov/sra/), accession PRJNA1280684.~~

~~3.6 Meteorological and Oceanographical datasets~~

~~To contextualize sediment deposition and transport dynamics, meteorological and oceanographic data were integrated with in situ observations, providing a comprehensive environmental framework during the study period. Atmospheric data were sourced from the MOLOCH model, a non-hydrostatic, convection-permitting numerical weather prediction system with 1.25 km resolution, producing 48-hour forecasts with hourly output (Davolio et al., 2017). Oceanographic and sea state data were obtained from the ADRIAC operational system, implementing the coupled COAWST model (ROMS and SWAN) with 1 km~~

resolution and 72-hour forecasts (Bressan et al., 2017). Model outputs are publicly available (https://dati-simc.arpae.it/opendata/adriac/). Complementary observational data include measurements from the TeleSenigallia marine weather station, equipped with an upward-looking ADCP (Ravaioli et al., 2016), and the ANCONA wave buoy of the Italian National Wave Buoy Network (ISPRA). Further technical details are provided in the Supplemental Material. Atmospheric fields are provided by the Numerical weather prediction model MOLOCH, developed and implemented at the Institute of Atmospheric Sciences and Climate of the National Research Council (CNR-ISAC). MOLOCH is a non-hydrostatic, fully compressible, convection-permitting model, implemented with a horizontal resolution of 1.25 km. The operational chain produces daily 48h forecasts with hourly resolution (http://www.isac.cnr.it/dinamica/projects/forecasts). Further details on the model can be found, e.g., in Davolio et al. (2017).

Oceanographic and sea state model data are provided by the ADRIAC operational system (Bressan et al., 2017), maintained by the by the Emilia-Romagna Regional Environmental Protection Agency (ARPAE). The system provides daily 72-hours forecast with hourly resolution and horizontal resolution of 1 km. The system is an implementation of the coupled model COAWST (Warner et al., 2010) over the Adriatic Sea, in particular with the ocean (ROMS) model and the wave (SWAN) model coupled two-way forced by the atmospheric model ICON. Forecast output are open and accessible at https://dati-simc.arpae.it/opendata/adriac/.

In addition to model data, sea-state and ocean currents observations have been collected at the marine weather station TeleSenigallia (see, e.g., Ravaioli et al., 2016), located near Senigallia (Ancona) 1 nm offshore at 12.5 m depth, equipped with an upward looking bottom mounted Teledyne Workhorse sentinel 300 KHz ADCP and maintained by the Institute for Marine Biological Resources and Biotechnology of the National Research Council (CNR-IRBIM), and at the ANCONA wave buoy, part of the Italian National Wave Buoy Network, courtesy of Italian Institute for Environmental Protection and Research (ISPRA, https://www.isprambiente.gov.it/en).

3.7 Statistical analyses

Statistical analyses were performed in Rstudio. Alpha diversity, represented as ASV richness, was calculated using the vegan package. Differences in richness values across sample types were evaluated using an ANOVA test (stats package, version

~~4.4.0), incorporating data from all transects. Post-hoc pairwise comparisons were performed using Tukey's HSD test to identify specific group differences. Beta diversity was assessed using non-metric multidimensional scaling (NMDS), comparing samples from different transects and examining variations based on their distance from the coast, using PERMANOVA analysis. To identify microbial biomarkers associated with river flood impact, a Linear Discriminant Analysis Effect Size (LEfSe) was performed. Finally, taxa associated with freshwater discharge were also identified as described in Massaccesi et al. (2025).~~

4. RESULTS

4.1 Spatial distribution of inorganic and organic components of sediments

Grain size analyses reveal a slight decreasing trend in particle size in the 2022 river flood deposit, distinctive from older deposits. Additionally, a progressive decrease in particle size is observed along all coast-normal transects (Fig. 4). Fine sand to coarse silt is primarily confined near the coastline and in less than 10 m water depth (Fig. 4), where sedimentary structures with oblique- and cross-lamination are present (Fig. 3). In contrast, further offshore muddy beds show an irregular surface at base and an overall fining up deposit (Figs. 3 and 4). The flood deposit shows relatively high bioturbation, few rounded pebbles, clasts and bioclasts content (Fig. 3). SEM imaging shows slightly sorted mudstone matrix with semi-consolidated clasts, detrital carbonate debris, and muscovite flakes (Fig. 3). Mudstone lithics can contain pyrite grains that likely were oxidized through outcrop weathering; limestone fragments are abundant (Fig. 3). Metal distribution in the flood sediment, reported in box and plots diagrams, shows concentrations much lower than the Italian permissible limits (Fig. 5). The flood deposit thin progressively seaward and are not present beyond the 15 m isobath (Figs. 3 and 4). Total Organic Carbon (TOC) increases by up to one order of magnitude in seaward sectors, reaching up to 1.2% (Fig. 4). Concurrently, $\delta^{13}C$ data indicate relatively higher OC_{Terr} concentrations, especially seaward of the Misa and Esino rivers (Fig. 4). Notably, fine sand laminations are observed only in sediments deposited prior to the 2022 event (Fig. 3). These earlier sediments exhibit lower TOC content and more depleted $\delta^{13}C$ values (Fig. 4). For all elements, pre-flood sediments record values slightly lower than the flood. Only two samples, 04 (Metauro3) and 05 (Metauro2) from the Metauro River transect, revealed two outliers (values exceeding 1.5 times

the interquartile range) for Cu, with concentrations of 50 and 56 mg kg^{-1}, respectively, however well below the threshold limit of 120 mg kg^{-1}. (Fig. 5).

As shown by the scatterplot diagrams (Fig. 6), sediment supplied from the Po River show high chromium and nickel concentrations, whereas relatively high calcium content typifies the Apennine provenance. Consistent with their geographic location close to the fluvial mouths of Apennine rivers, almost all samples plot in the field of Apennine composition, with the sole exception of sample 16 (collected >15 km from the coast), which is characterized by lower Ca and higher Cr concentrations and likely reflects Po River influence via the longshore currents. In general, there is strong overlap in composition between flood and pre-flood samples (Fig. 5), suggesting continuous supply from the Apennine rivers, regardless of the competence of individual flood events (Fig. 6).

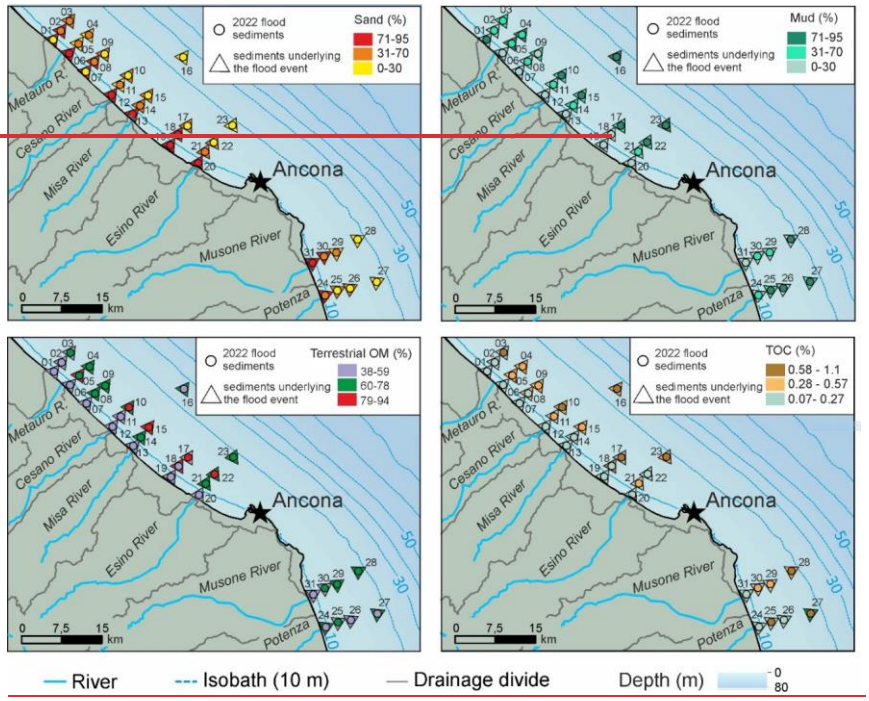

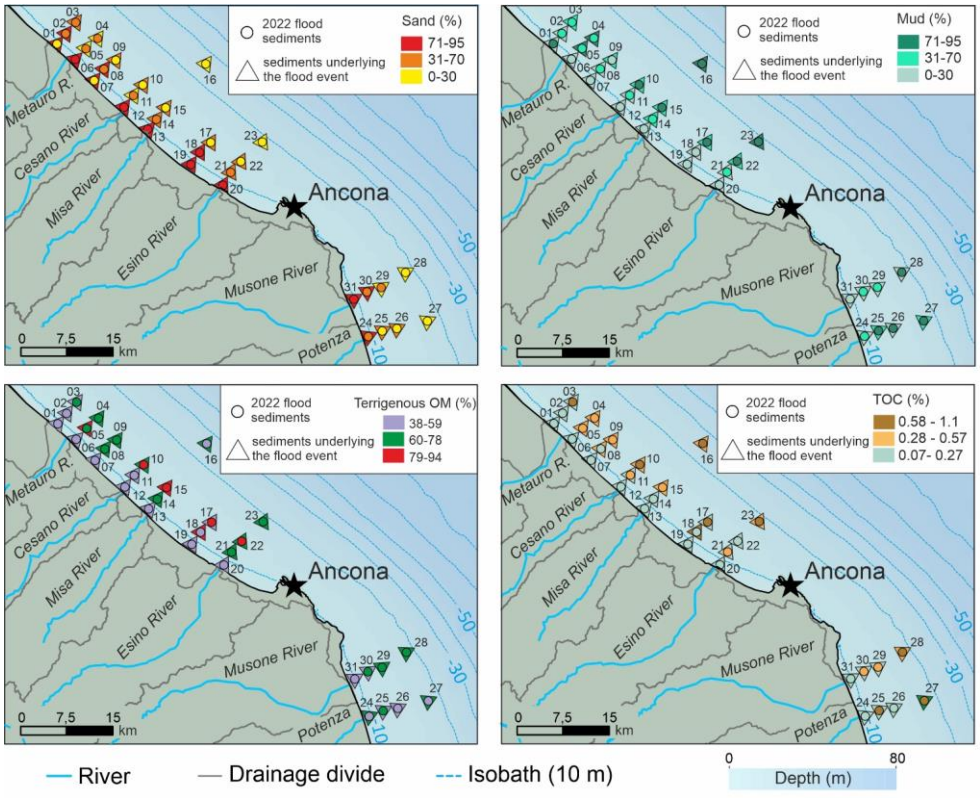

Figure 4: Sediment properties and geochemical parameters in the coastal, prodelta and offshore area of Marche region. Maps show distributions of sand (%), mud (%), ~~$\delta^{13}C$~~terrigenous organic matter concentration (OMterr ~~%~~%), and total organic carbon (TOC, %) at sampling stations. Colored circles represent measured values for both samples of the river flood sediments deposited in 2022 (~~small~~ circles) and in older underlying sediments (~~large circle~~triangles)~~.~~ background shading indicates ~~satellite-derived chlorophyll-a concentration (mg m^{-3}) as a proxy for surface productivity~~bathymetric variations (~~.~~ ~~D~~dashed lines are 10 m isobaths); rivers and drainage divides are also shown.

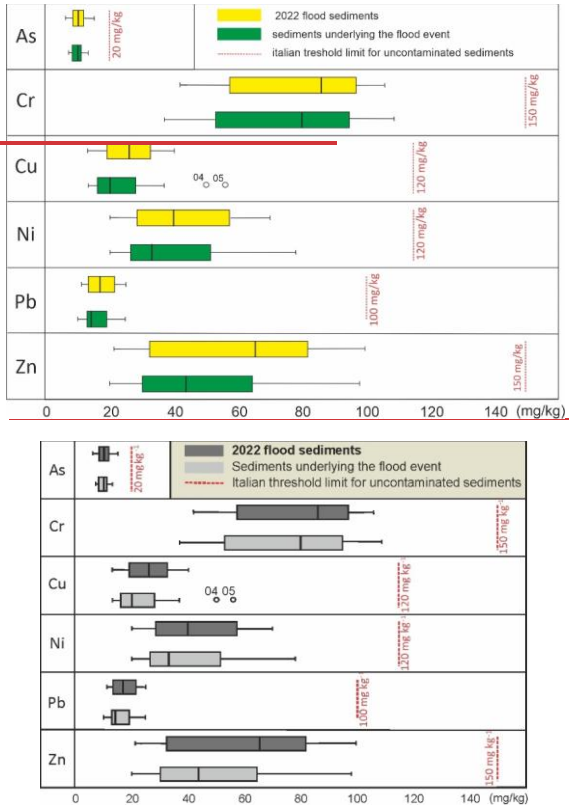

445 **Figure 5: Boxplots of metal concentrations (mg kg^{-1}) in river flood sediments deposited in 2022 (~~Top~~dark grey boxes) and in older underlying sediments (~~Bottom~~light grey boxes) for As, Cr, Cu, Ni, Pb, and Zn. ~~Yellow and green boxes represent top and bottom sediments, respectively.~~ Dashed red lines indicate sediment quality guideline thresho lds. Outliers are shown as open circles.**

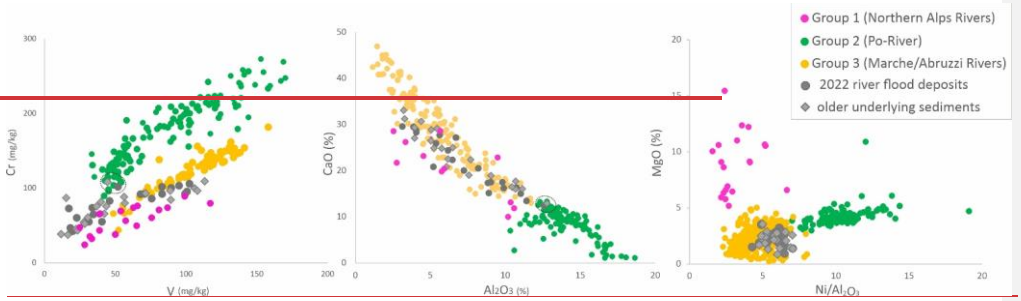
Group 1 (Northern Alps Rivers)
Group 2 (Po-River)
Group 3 (Marche/Abruzzi Rivers)
2022 river flood deposits
older underlying sediments
Cr (mg/kg)
V (mg/kg)
CaO (%)
Al2O3 (%)
MgO (%)
Ni/Al2O3

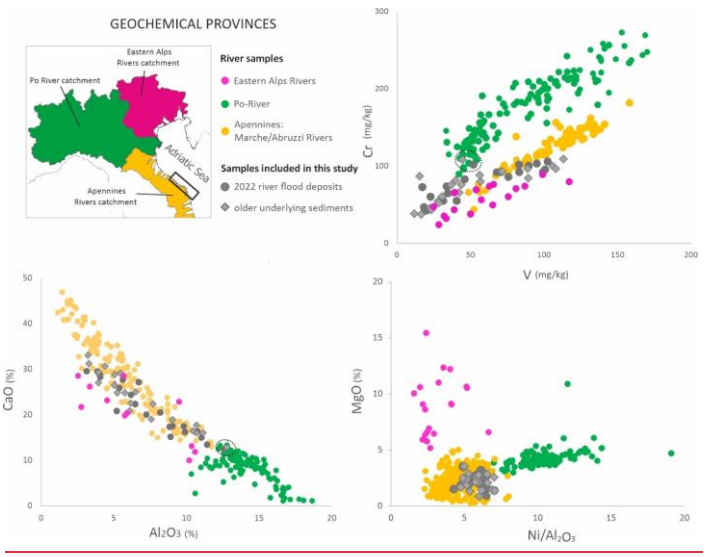
GEOCHEMICAL PROVINCES
Eastern Alps Rivers catchment
Po River catchment
Apennines Rivers catchment
Adriatic Sea
River samples
Eastern Alps Rivers
Po-River
Apennines: Marche/Abruzzi Rivers
Samples included in this study
2022 river flood deposits
older underlying sediments
Cr (mg/kg)
V (mg/kg)
CaO (%)
Al2O3 (%)
MgO (%)
Ni/Al2O3

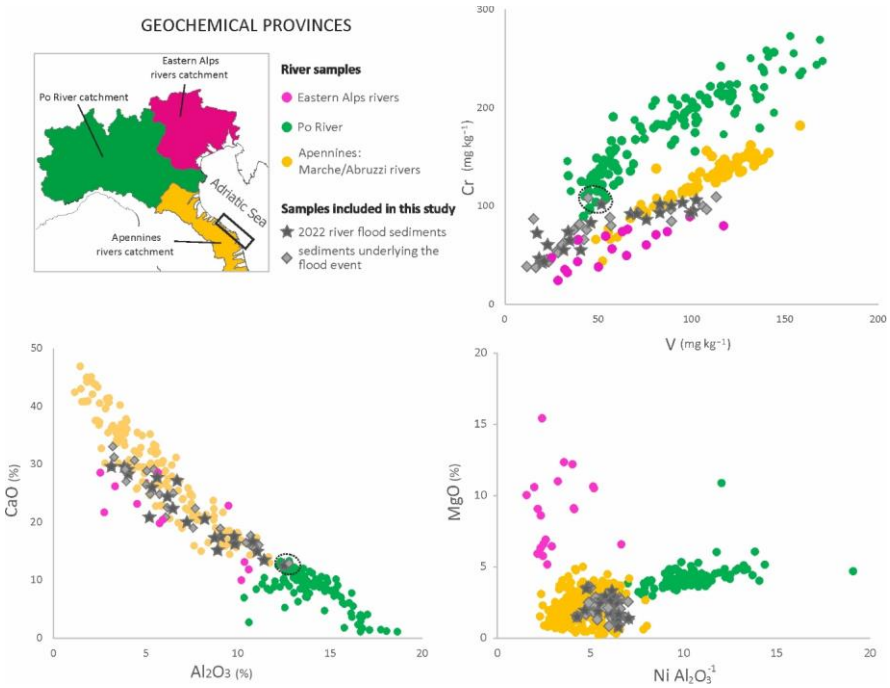

Figure 6: Main geochemical provinces of northern and central Adriatic Sea as documented in Amorosi et al., 2022, with the study area outlined (black box), along with ~~-S~~scatterplot diagrams of selected geochemical indicators of sediment provenance. The geochemical composition of sediment from the Po River catchment has high Cr and Ni/Al_2O_3 and low CaO. ~~S~~Sediment from ~~the~~the ~~-~~Eastern Alps catchment ~~(Group 1)~~ exhibits high CaO and MgO values, along with low Cr and Ni/Al_2O_3. ~~Sediment from the Po River (Group 2) has low CaO and high Cr and Ni/Al_2O_3.~~ Sediment from Marche/Abruzzi Apennines ~~(Group 3)~~ shows high CaO and low Cr, Ni/Al_2O_3 and MgO. Samples analyzed in this study (grey dots and diamonds) are consistent with an Apennine origin of the sediment from the Marche/Abruzzi catchments except for samples from site 16 (black dashed line) which can be related to a mixed Apennine-Po River provenance.

4.2 Polycyclic Aromatic Hydrocarbons

Total PAH concentrations differed between the various sampling sites, with the highest values found at the site sampled offshore of the Misa River (Misa3, 141 ng g^{-1} dw), the river most affected by the flood event in the Marche Region, and lower values at the sampling site offshore of the Potenza River (Potenza 3, 15 ng g^{-1} dw), less impacted by the flood event. In general, a consistent trend is observed across the sampled transects, with higher values at offshore sites compared to coastal ones (Fig. 7). The most common PAHs at coastal sites are acenaphtylene and fluoranthene, while the most common PAHs at the offshore sites are acenaphthylene and phenanthrene. In all sediment samples analyzed, HMW PAHs were below 5 ng g^{-1} dw (Fig. 7). Statistically significant differences (Mann-Whitman, p >0.05) between coastal and offshore samples were recorded for all individual PAHs, except for naphthalene, acenaphthene, fluorene, and fluoranthene. Notably, the Misa River transect showed the largest difference between the offshore site (141 ng g^{-1} dw) and the coastal site (25 ng g^{-1} dw). Higher values in the open sea compared to the coastal one were also observed in the Cesano (69 vs. 27 ng g^{-1} dw) and Metauro (50 vs. 18 ng g^{-1} dw) river transects. A discrepancy in this pattern was observed in the Potenza River transect, where the values at the offshore site were lower than those at the coastal site (15 vs. 43 ng g^{-1} dw). Some transects showed no significant difference between offshore and coastal sites, such as the transects at station A (52 vs. 47 ng g^{-1} dw) and station C (30 vs. 31 ng g^{-1} dw). The concentrations of total PAHs (ng g^{-1} dw) in surface sediment samples, both offshore and coastal, are shown in Table S1. Figure S1 shows the percentage contribution of each individual PAH to their total amount. In most of the marine sediment analyzed, LMW compounds dominate, accounting for over 50% of the total PAHs. An exception is the sediment sample collected near the mouth of the Potenza River (Potenza1), where the predominant PAH is fluoranthene, a four-ring aromatic compound considered HMW, which accounts for more than 40% of the total PAHs.

Investigated PAH isomer indicators such as *anthracene/(anthracene + phenanthrene)*, *fluoranthene/(fluoranthene + pyrene)* and *benz(a)anthracene /(benz(a)anthracene + chrysene*) show that the dominant sources of the investigated PAHs were primarily combustion-related (Fig. 8). Samples close to the coast, Potenza1 and, in smaller amounts, Cesano1 and C1 sites, show a strong dominance of PAHs with pyrogenic sources. In all other cases, *LMW/HMW* and *ΣCOMB/ΣPAHs* ratios also indicated a petrogenic sources for all samples, particularly in the sediments collected north of the flood event, and far from the

coast (A1, Metauro3 and B3). Otherwise, Potenza1 site confirmed its pyrolytic origine. Particularly, A3 and Musone3 sites were more closely related to a petrogenic origin than a pyrogenic one (Fig. 8).

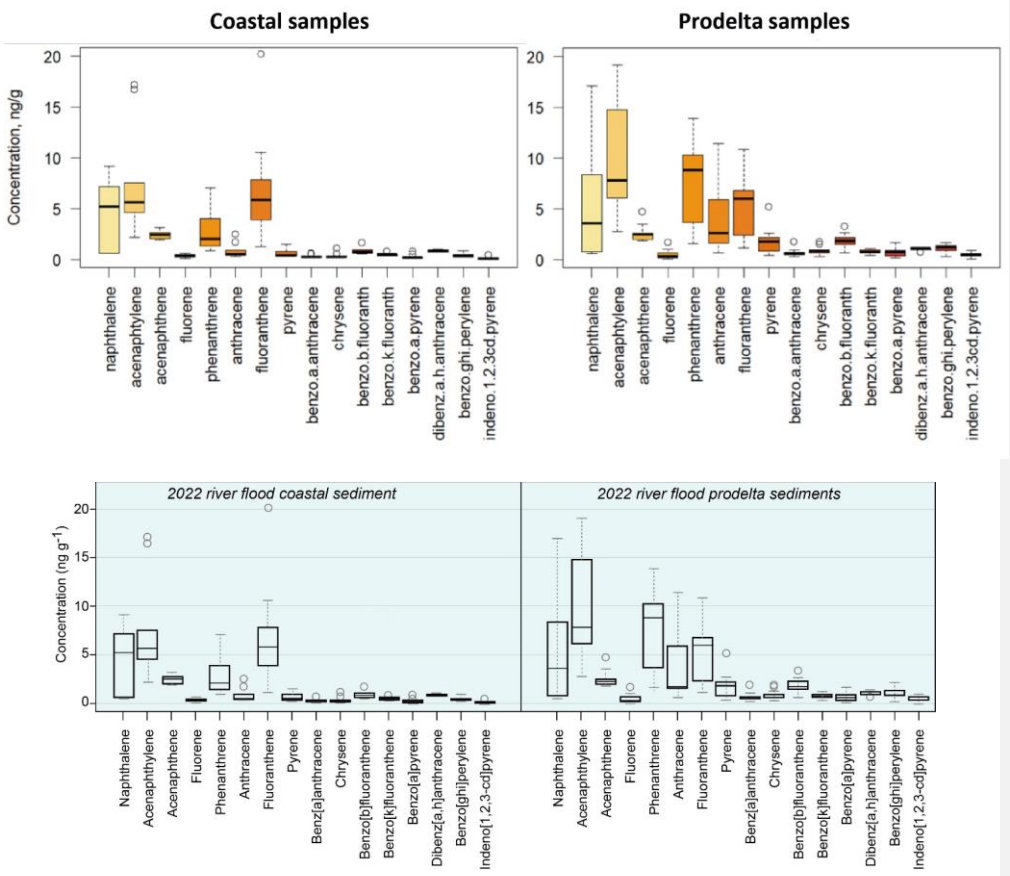

490 **Figure 7: Concentrations (ng g^{-1} dry weight) of main PAHs in the 2022 river flood sediments. Boxplots show the distribution of individual PAH compounds, highlighting differences in composition and levels between nearshore and prodelta sectors. Outliers are shown as open circles.**

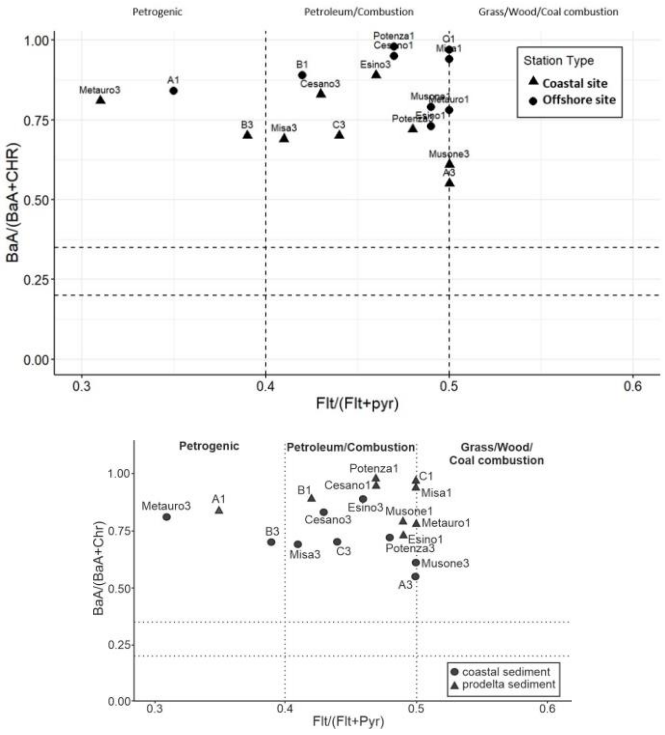

Figure 8: Diagnostic ratio plot of PAHs using Flt/(Flt+Pyr) vs. BaA/(BaA+Chr) to infer the origin of organic matter in the 2022 river flood sediments. Coastal sites (triangle) and prodelta sites (circle) are classified into petrogenic, petroleum/combustion, and biomass/coal combustion sources based on threshold values (dashed lines) from literature.

4.3 Poly- and Perfluorinated alkyl substances

Among the 17 investigated PFASs, only six compounds were detected in the sediment samples: four belonging to the traditional target group and two fluorotelomer classified as next-generation PFASs. All other PFASs were below the Method Quantification Limits (MQLs; Fig. 9). Furthermore, a large proportion of the samples corresponding to the deeper, pre-flood sediment layers, showed no detectable PFAS contamination. Considering sediments deposited during the 2022 river flood,

6:2FTS remained the predominant compound, followed by an 8:2FTS contamination of lesser extent. These sulfonated fluorotelomers are considered next-generation PFASs, commonly used as replacements for legacy compounds due to regulatory restrictions, and are known for their high environmental persistence (Field and Seow, 2017). 6:2FTS was detected at consistently higher concentrations than those in the corresponding pre-flood layers (approximately two orders of magnitude greater), with values ranging from 0.203 to 86.10 ng g^{-1} dw. This compound was detected both offshore and nearshore, with a general decreasing trend observed along almost all coastal-to-offshore transects. 8:2 FTS was also detected in the surface sediments, though at lower concentrations (0.210-0.439 ng g^{-1} dw), and only in transects A (offshore), Metauro River and B (both sampling points), and in the nearshore sampling point of the Misa River transect (Fig. 9).

Perfluorohexanoic acid (PFHxA), perfluorooctanoic acid (PFOA), and perfluoroundecanoic acid (PFUnA) were each detected only in one sample, collected from the seaward sector of the Metauro River transect, at concentrations of 0.120, 0.127, and 0.208 ng g^{-1} dw, respectively. Perfluorooctanesulfonic acid (PFOS), the only perfluorinated sulfonic acid (PFSA) identified, was detected exclusively in the seaward sector of the Esino River transect at a concentration of 0.052 ng g^{-1} dw, suggesting a very limited distribution of this compound across the study area. No PFASs were detected in transects associated to the Musone and Potenza rivers, both located South of the Ancona Promontory (Fig. 9).

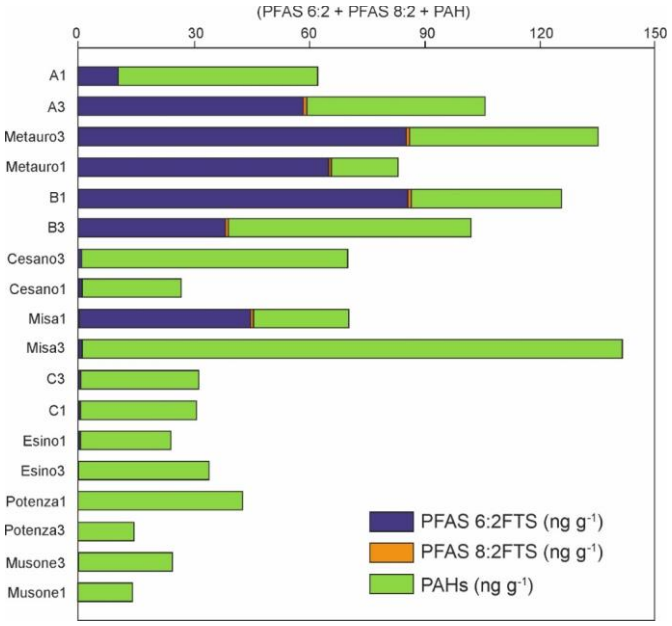
(PFAS 6:2 + PFAS 8:2 + PAH)
0
30
60
90
120
150
A1
A3
Metauro3
Metauro1
B1
B3
Cesano3
Cesano1
Misa1
Misa3
C3
C1
Esino1
Esino3
Potenza1
Potenza3
Musone3
Musone1
PFAS 6:2FTS (ng g-1)
PFAS 8:2FTS (ng g-1)
PAHs (ng g-1)

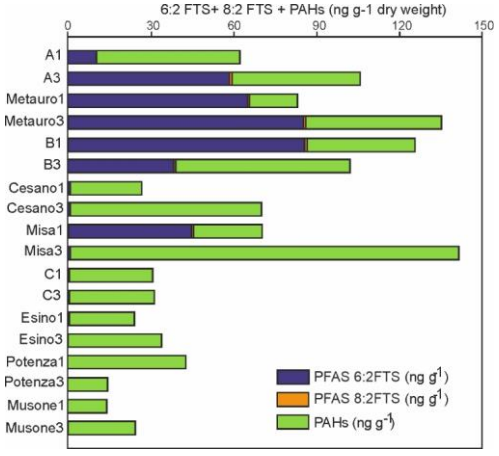
6:2 FTS+ 8:2 FTS + PAHs (ng g-1 dry weight)
0
30
60
90
120
150
A1
A3
Metauro1
Metauro3
B1
B3
Cesano1
Cesano3
Misa1
Misa3
C1
C3
Esino1
Esino3
Potenza1
Potenza3
Musone1
Musone3
PFAS 6:2FTS (ng g-1)
PFAS 8:2FTS (ng g-1)
PAHs (ng g-1)

Figure 9: Stacked bar chart showing the relative abundance of 6:2 FTS, 8:2 FTS (PFASs), and total polycyclic aromatic hydrocarbons (tot. PHAs) across all sampling locations.

4.4 Microbial communities' description

Microbial diversity increased progressively with distance from shore. Statistical analyses revealed significantly lower Shannon diversity values in samples collected closer to the coast (ANOVA, $p < 0.01$), particularly compared to offshore samples (Tukey's test $p < 0.01$). A similar, though not statistically significant, trend was observed for richness values (Fig. 10A). Beta diversity analyses (Fig. 10B) revealed a clear spatial gradient in benthic prokaryotic community structure along the coast-to-offshore transects (ANOSIM $p = 0.001$, $R = 0.6$), largely reflecting variations in sediment grain size, with the exception of samples from the Musone River. Offshore samples formed a distinct cluster further composed by two subgroups, one associated with silt and on one with clay, TOC and TN (Fig. 10B).

All samples were dominated by Gammaproteobacteria (average $26.39 \pm 2.61\%$), Bacteroidia ($10.14 \pm 3.35\%$), Thermoanaerobaculia ($7.49 \pm 2.42\%$), and Planctomycetes ($7.02 \pm 1.41\%$), with noticeable variability observed in their relative abundances from coastal to offshore sites (Fig. S2).

LEfSe analysis (Fig. 10C) was conducted to identify microbial taxa significantly associated with sample groups defined by their distance from the coast and flood impact. Coastal samples were significantly ($p < 0.001$) enriched in Thermoanaerobaculaceae, Pirellulaceae, and Woeseiaceae (genus *Woesia*), whereas prodelta samples were characterized by the Desulfobulbaceae. Offshore samples displayed a higher relative abundance of Vicinamibacteria, Flavobacteriaceae and Cyclobacteriaceae (Fig. 10C).

As an additional analysis to trace riverine influence, freshwater-indicator taxa were searched in the analysed samples. Results showed that these taxa (i.e. Flavobacterium, Variovorax) were retrieved in offshore samples associated with clay, TOC and TN (Supplementary Fig. S3), whereas they were largely absent or rare in coastal and silt-associated offshore sites.

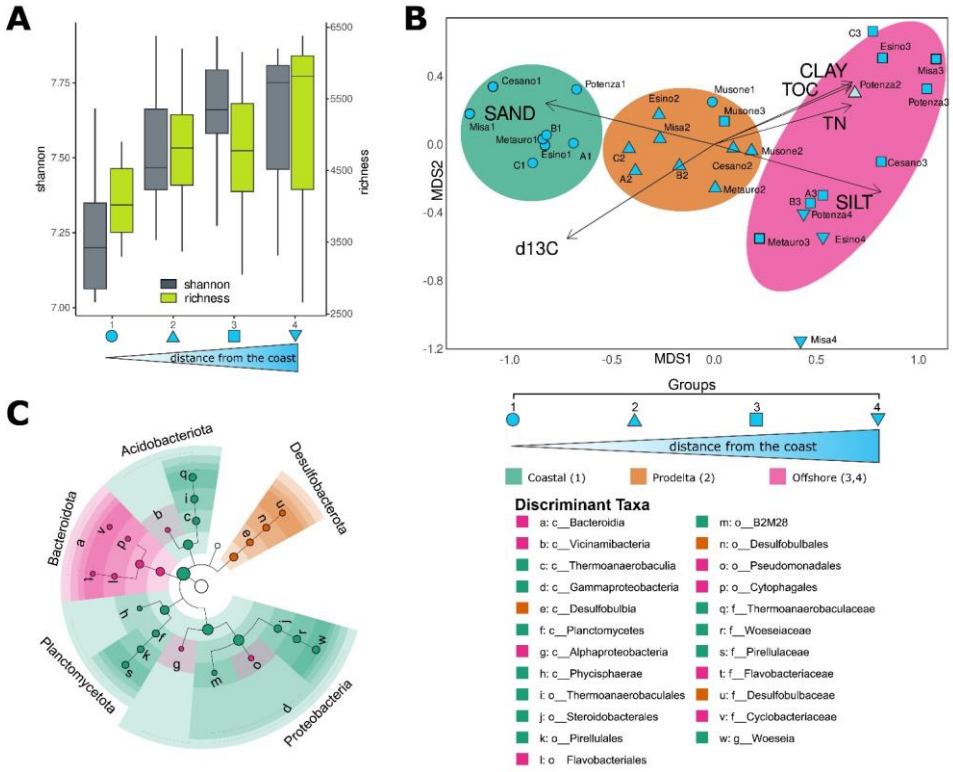
A
shannon
richness
distance from the coast
B
SAND
CLAY
TOC
TN
SILT
d13C
MDS1
MDS2
Groups
distance from the coast
Coastal (1)
Prodelta (2)
Offshore (3,4)
Discriminant Taxa
a: c__Bacteroidia
b: c__Vicinamibacteria
c: c__Thermoanaerobaculia
d: c__Gammaproteobacteria
e: c__Desulfobulbia
f: c__Planctomycetes
g: c__Alphaproteobacteria
h: c__Phycisphaerae
i: o__Thermoanaerobaculales
j: o__Steroidobacterales
k: o__Pirellulales
l: o__Flavobacteriales
m: o__B2M28
n: o__Desulfobulbales
o: o__Pseudomonadales
p: o__Cytophagales
q: f__Thermoanaerobaculaceae
r: f__Woeseiaceae
s: f__Pirellulaceae
t: f__Flavobacteriaceae
u: f__Desulfobulbaceae
v: f__Cyclobacteriaceae
w: g__Woeseia
C
Acidobacteriota
Desulfobacterota
Bacteroidota
Planctomycetota
Proteobacteria

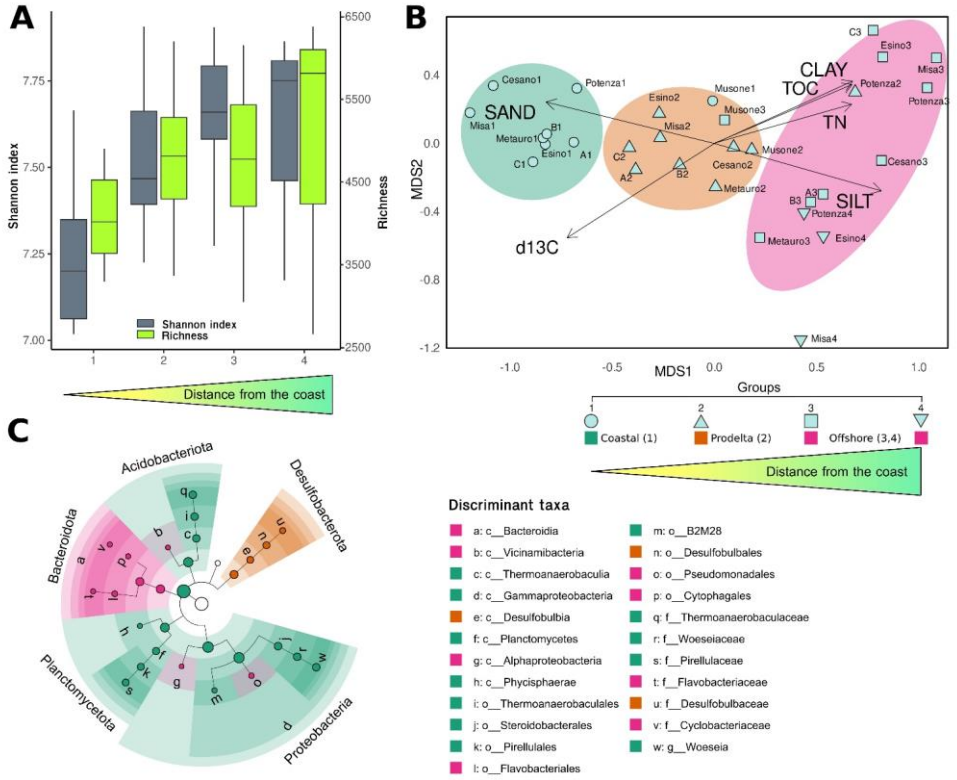

Figure 10: Microbial community structure and diversity across the coastal-sea transect of the 2022 river flood sediments. Box plots of Shannon diversity and ASV richness (A) indices, clustered by distance from the coast and river impact. (B) Non-metric Multidimensional Scaling (nMDS) ordination based on a Bray-Curtis dissimilarity matrix (Stress = 0.20); shapes indicate distance clusters, and ellipses represent 95% confidence intervals. (C) LEfSe cladogram showing differentially abundant taxa (p <0.001) among clusters from the nMDS; each dot represents a discriminant taxon, colored by the cluster in which it is most abundant.

4.5 Meteo-ocean conditions

Oceanographic conditions along the coast during the flooding event were quite calm. This is true until September 17th, when a low-pressure system rapidly moving across the Adriatic Sea resulted (locally along the coast of the Marche Region) in gale-force northeasterlies during the afternoon, rapidly vanishing a few hours later. The evolution can be followed on Figure 11, showing the onset of northeasterlies in the early morning (Fig. 11a), directly impacting the coast at noon (Fig. 11b), finally rotating as northwesterly in the evening (Fig. 11c). Data collected offshore Senigallia and in Ancona show a rapid intensification of the sea state (Fig. 11d) with significant wave height of, respectively, 3 and 4.5 m, with a marked peak and rapidly decreasing later on. Data from the TeleSenigallia ADCP also show intensification of a longshore (ca. 120°, i.e., toward south-east, see Fig. 11f) currents with peak during the windstorm of 1 $m\,s^{-1}$ at the surface and 0.7 $m\,s^{-1}$ near bottom (Fig. 11e). As for the sea state, current intensity dropped quickly after a few hours. Ocean model data (Fig. 11g, h, i) provide a larger picture with the same features: rough sea state and accelerated coastal current at noon rapidly leaving the area toward the southern Adriatic following the disturbances. After a few hours, the Marche Region coastline turned back to calm sea state conditions and weakened coastal current. Although this windstorm did not last long, it followed closely the flooding event. Thus, it is relevant to take this into consideration while understanding the sediment transport right after the discharge.

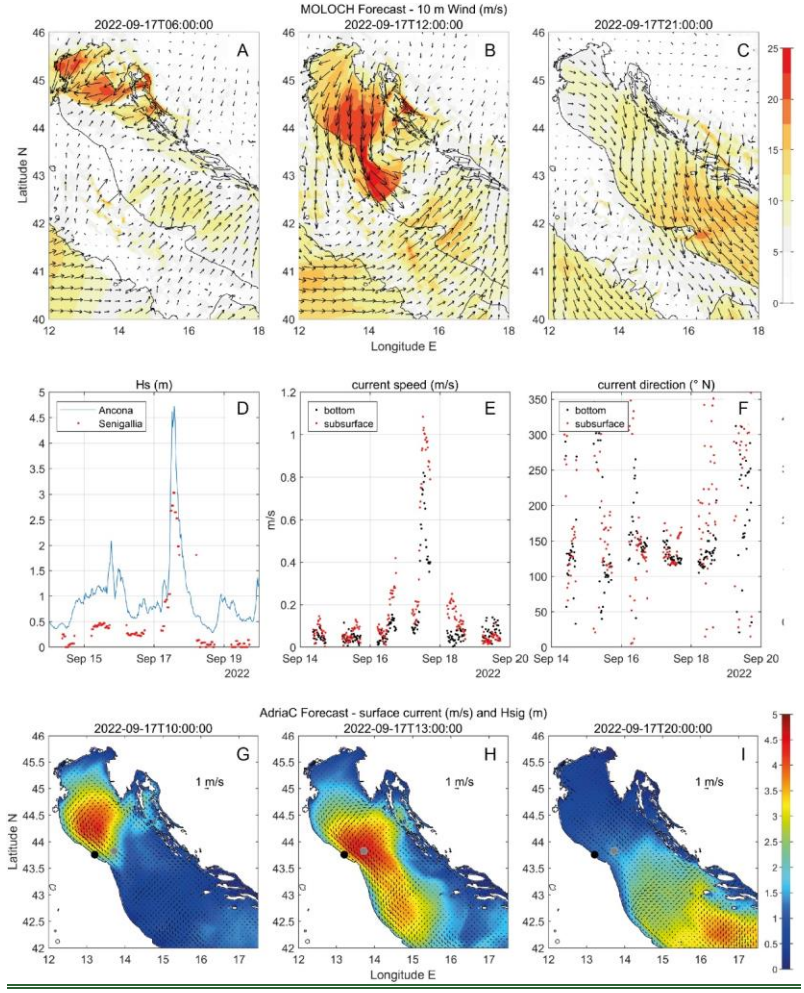

565

Figure 11: 10 m wind (m s^{-1}) MOLOCH forecast valid time 17 September 2022 (A) 06:00 UTC, (B) 12:00 UTC, and (C) 21:00 UTC; (D) significant wave height (m) measured at Ancona (blue line) and Telesenigallia (red dots), (E) ocean currents speed (m s^{-1}) measured by TeleSenigallia ADCP, along with (F) currents direction (degree, 0 N, flowing

~~toward); ADCIRC forecast for significant wave height (m, color coded) and surface currents (black arrows) valid time~~ ~~17 September (C) 10:00 UTC, (H) 13:00 UTC, (I) 20:00 UTC. The black filled circle indicates TeleSenigallia marine station position. The gray filled circle indicates Ancona wave buoy position. Technical details on the source datasets can be found in the supplementary material.~~

5. DISCUSSIONS

The sedimentological evidence of fine sediment deposition, combined with contaminant hotspots and shifts in microbial community composition, reveals an interconnected system where physical transport processes directly modulate chemical and biological responses. This integrative framework, synthesized in Fig. 12, enables a more holistic understanding of the short-term sedimentary and ecological responses to an extreme hydrological disturbance. In this framework, fine-grained flood deposits act as the primary coupling mechanism between physical forcing, contaminant redistribution, and biological responses

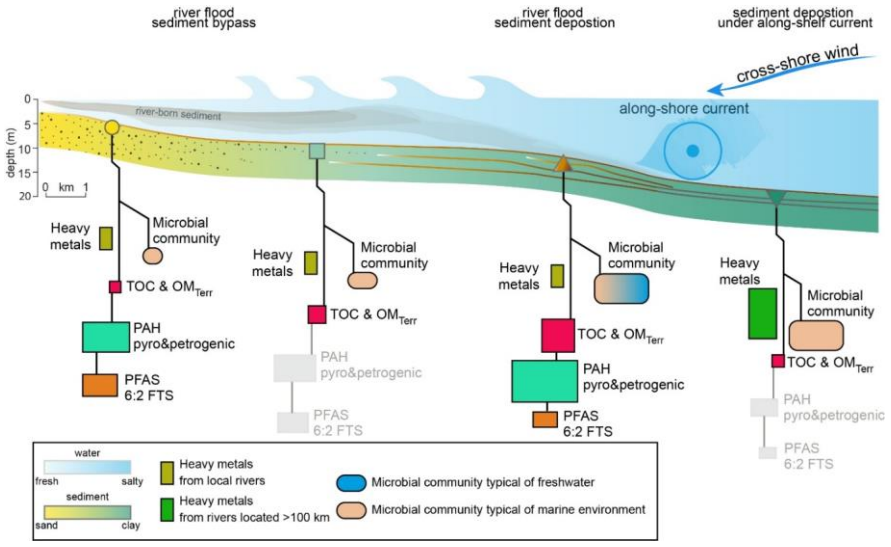

Figure 12~~1~~1: Conceptual model of sediment transport, contaminant distribution, and microbial community variation along a coastal transect where sediment and associated contaminants are transported and deposited across a coastal gradient under the influence of riverine input, wave action, and along-shelf currents. During flood events, high-energy river flows can bypass the wave-influenced nearshore zone and deliver sediments offshore, where they are preferentially deposited in the prodelta. This distal accumulation occurs in areas where the energy of the plume is reduced and flow is laterally confined by the prevailing along-shelf current. The size of the shapes reflects the relative abundance of each contaminant, while the size of the microbial community symbol reflects diversity rather than quantity. Colors differentiate sources (e.g., local vs. remote rivers) and environmental influences (e.g., fresh vs. salt water).

5.1 ~~Sedimentary dynamics and~~M~~m~~eteorological-oceanographic controls on river flood deposits~~The ephemeral nature of river flood deposits~~

The spatial distribution and preservation of sediment deposits from the September 2022 flood are strongly controlled by the interplay between fluvial inputs and coastal meteo-oceanographic dynamics (Fig. 12~~1~~1) ~~(Fig. 12)~~. Depositional processes govern sediment transport pathways, ~~and~~ grain size, and depositional environments, with finer sediments more prone to ~~offshore~~ deposition and preservation in the prodelta, while coarser sediments dominate nearshore zones subject to continuous resuspension. Also, nearshore zones (~5 m water depth) adjacent to river mouths exhibit limited sediment retention due to intense wave-induced resuspension and alongshore transport driven by coastal currents (Palinkas & Nittrouer, 2006; Puig et al., 2007; Pellegrini et al., 2024). ~~On September 17th, t~~The rapid intensification of northeasterly ~~Bora~~ winds during the final phase of the flooding ~~generated~~ intensified ~~significant wave heights of 3–4.5~~cross shore sea state ~~m~~ and alongshore currents (~~ex~~ Fig. 11~~2~~2) ~~up to 1 m s^{-1} offshore Senigallia and Ancona (Fig. 11d,e),~~ increasing bed shear stresses sufficient to erode and remobilize fine flood-derived sediments ~~(Fain et al., 2007; Friedrichs & Scully, 2007)~~. These dynamics caused nearshore resuspension and advective southward displacement of sediments, effectively limiting offshore dispersion beyond the 15 m isobath (Fig. 12~~1~~1) ~~(Fig. 12)~~. As a result, the nearshore zone acts as a high-energy bypass area where sedimentary, chemical, and biological flood signals are rapidly diluted or erased. The sandy nearshore sectors are thus subject to continuous

ha formattato: Colore carattere: Azzurro
ha formattato: Colore carattere: Azzurro
ha formattato: Non Evidenziato
ha formattato: Colore carattere: Automatico

remobilization, likely facilitating bypass of riverine plumes and ~~restricting sediment accumulation nearshore~~focused erosion, consistent with previous findings (Palinkas & Nittrouer, 2006; Cattaneo et al., 2007; Fain et al., 2007; Friedrichs & Scully, 2007; Traykovski et al., 2007; Pellegrini et al., 2024). ~~The brief but intense Bora event was therefore pivotal in shaping sediment transport and deposition during the flood.~~

In contrast, more distal prodelta environments (10–15 m water depth) provide more favorable conditions for preservation of flood deposits (Fig. ~~12~~11). Here, sedimentary features such as rip-up clasts of semi-consolidated mud indicate erosion of previously deposited fine sediments at the river mouth, followed by bypass and deposition in the prodelta, consistent with depositional patterns described for the ~~Pescara River prodelta~~central Adriatic Sea (Pellegrini et al., 2021, 2024). ~~Oceanographic~~ Hydrodynamics model and in-situ data support this interpretation, showing a rapid but transient intensification of coastal currents in response to the ~~Bora~~ windstorm, ~~which weakened within hours (Fig. 11g–i), highlighting~~suggestive of dynamic interactions between river discharge and marine hydrodynamics over short timescales. Similar sediment transport and current patterns linked to northeasterlies (locally known as Bora winds) ~~Bora winds~~ and the Western Adriatic Coastal Current (WACC) have been documented in previous studies (Book et al., 2007; Wang & Pinardi, 2002; Sherwood et al., 2004; Palinkas et al., 2007; Harris et al., 2008; Benincasa et al., 2019; Signell et al., 2010; Vona et al., 2025). ~~During the 2022 event, the Bora windstorm generated offshore surface waves exceeding 4 m in significant height (Fig. 11d) with a peak period of ~9 s, rapidly invigorating the coastal current (Fig. 11e), increasing bed shear stress and alongshore transport. However~~On the other hand, the short duration of the windstorm most likely limited southward sediment displacement, effectively trapping suspended particles within the prodelta and causing a spatially restricted, temporary accumulation of river-derived material (Fig. ~~12~~11). Notably, only samples collected farther offshore and unaffected by the 2022 flood show sediment compositions attributable to the Western Alps (Amorosi et al., 2022 for a review), indicating that river-borne sediment was hydrodynamically confined by the WACC during the event (Fig. ~~12~~11). This evidence demonstrates that even extreme flood events can leave subtle and stratigraphically limited signals in shelf sediments, raising concerns about detecting high-magnitude river floods in marine sedimentary records.

~~The sedimentary signature of river floods changes markedly with distance from the shoreline. In very shallow areas adjacent to river mouths (approximately 5 m water depth), flood-related deposits are more difficult to identify. These nearshore sectors~~

Formattato: Interlinea: doppia

~~are dominated by sandy sediment and subjected to remolding through high-energy processes including hyperpycnal flow bypassing, wave-induced resuspension, and alongshore transport by coastal currents (Palinkas & Nittrouer, 2006; Cattaneo et al., 2007; Puig et al., 2007; Traykovski et al., 2007; Pellegrini et al., 2021, 2024). Additionally, coastal storm waves generate bed shear stresses sufficient to erode and remobilize fine-grained sediment (Fain et al., 2007; Friedrichs & Scully, 2007; Traykovski et al., 2007; Pellegrini et al., 2021, 2024). These conditions facilitated the bypass of riverine plumes from Apennine catchments during the 2022 flood and limited the deposition of flood-derived sediment in the nearshore zone (Fig. 12). In contrast, more distal prodelta environments (10–15 m water depth) offer a more favorable setting for the preservation of flood deposits (Fig. 12). Here, sedimentary features such as rip-up clasts of semi-consolidated mud indicate erosion of previously deposited fine-grained sediments. These characteristics are consistent with depositional patterns previously described for the Pescara River prodelta (Pellegrini et al., 2024). The 2022 flood layers also exhibit a distinct $\delta^{13}C$ signature indicative of terrestrial origin (Tesi et al., 2007; Bao et al., 2016; Broder et al., 2018; Hage et al., 2022; Pellegrini et al., 2021; Nogarotto et al., 2023), along with elevated concentrations of anthropogenic pollutants (Frapiccini et al., 2024; Fig. 12). The PAHs concentrated in the prodelta sector, suggesting that such hydrophobic organic contaminants reflect the transport dynamic of organic-rich riverine clays, following a similar dispersal pathway, as suggested also in other prodelta systems (e.g. Roussiez et al., 2006; Bouloubassi et al., 2012). It is also important to highlight that in a few cases the PAH content in the Adriatic prodelta deposits is five times higher than the nearshore samples (e.g. Misa River), highlighting the role of river flood in creating focused pollutant hotspots (Fig. 12). Such considerations are of great concern from the environmental and ecological viewpoints because coastal ecosystems are directly exposed to sediment-bound contaminants, which, with increasing extreme events, particle delivery will be enhanced during extreme hydro-meteorological events such leading to river floods.~~

~~Despite the severe damage and well-documented hydrological impact of the September 2022 flood event on land, its offshore sedimentary expression proved ephemeral. Our data show that flood-related deposits were largely confined to the nearshore zone, within the 15 m isobath, and in many cases were spatially discontinuous and patchily preserved. This limited offshore signature can be attributed to the interplay between concurrent high river discharge and high-energy meteo-marine conditions (Fig. 11). We hypothesize that reduced wave-induced shear stress in the prodelta sector allows for the partial settling of suspended particles, while alongshore currents advect the sediment plume to the south, preventing offshore diffusion (Fig. 12).~~

Similar sediment transport has been documented form satellite observations (Benincasa et al., 2019; Vona et al., 2025). While northeasterlies (Bora winds, see e.g, Signell et al., 2010) have relatively short fetch blowing perpendicular to the Adriatic Sea major axis, they can be severe enough to generate energetic waves (Pomaro et al. 2017). It is also well established that Bora windstorms in the Adriatic Sea enhance the Western Adriatic Coastal Current (WACC; e.g., Book et al. 2007) leading to alongshore sediment transport (Wang & Pinardi, 2002; Sherwood et al., 2004; Palinkas et al., 2007; Harris et al., 2008; Benincasa et al., 2019). During the 2022 event, the windstorm of September 17th was strong enough to produce offshore surface waves more than 4 m in significant wave height (Fig. 11d) and relatively long peak period (9 s, not shown), thus with significant impact on sediment remobilization when approaching the coast (Fig. 12). The rapid invigoration of the coastal current (Fig. 11e) intensified bed shear stress and alongshore transport. The relatively short duration of the windstorm limited the southward displacement of sediment, effectively trapping suspended particles along the prodelta. The result is a temporary, spatially limited accumulation of local river-derived material within a narrow coastal sector. Notably, the only samples displaying a composition attributable to the Wester Alps (Amorosi et al., 2022) are those collected most offshore and unaffected by the 2022 flood. In this context, the river-borne sediment appears deflected and hydrodynamically confined by the WACC (Fig. 12). This evidence indicates that even extreme flood events may leave only a subtle and stratigraphic signal confined to the shallow-marine record, raising concern about the detectability of high-magnitude events in shelfal sedimentary archives.

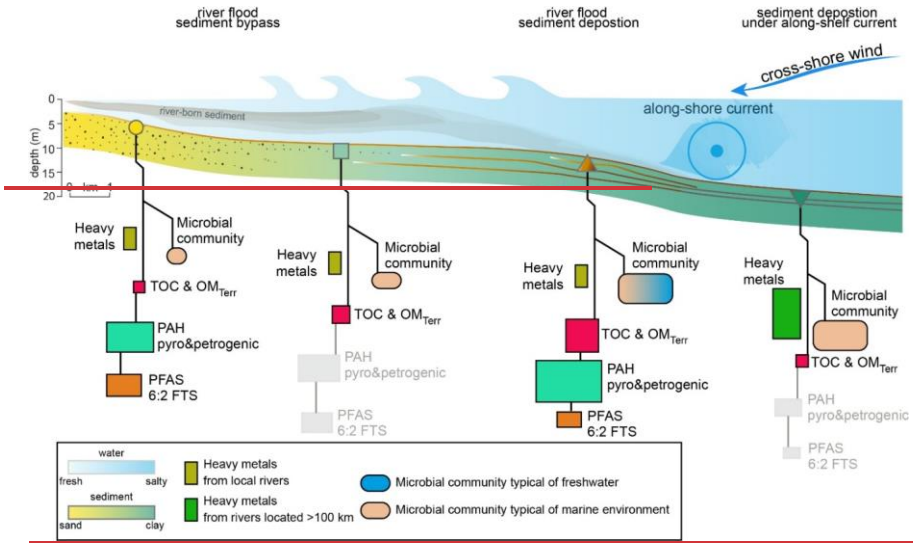

~~**Figure 12: Conceptual model of sediment transport, contaminant distribution, and microbial community variation along a coastal transect where sediment and associated contaminants are transported and deposited across a coastal gradient under the influence of riverine input, wave action, and along-shelf currents. During flood events, high-energy river flows can bypass the wave-influenced nearshore zone and deliver sediments offshore, where they are preferentially deposited in the prodelta. This distal accumulation occurs in areas where the energy of the plume is reduced and flow is laterally confined by the prevailing along-shelf current. The size of the shapes reflects the relative abundance of each contaminant, while the size of the microbial community symbol reflects diversity rather than quantity. Colors differentiate sources (e.g., local vs. remote rivers) and environmental influences (e.g., fresh vs. salt water).**~~

5.2 Pollutant distribution patterns reflecting fluvial and oceanographic processes

Understanding the origin and behavior of contaminants in marine sediments is crucial for assessing environmental and human-health risks, as well as for implementing effective coastal management strategies (Neff et al., 2005; Di Lorenzo et al., 2020;

Pizzini et al., 2021; Pellegrini et al., 2023; Trincardi et al., 2023). Given the hydrodynamic confinement and selective deposition processes described above, contaminant distributions following flood events are expected to be spatially heterogeneous rather than uniformly dispersed. In this study, the spatial heterogeneity of sediment-bound contaminants, including Polycyclic Aromatic Hydrocarbons (PAHs) and Poly- and Perfluorinated Alkyl Substances (PFASs), reflects differential transport and depositional pathways shaped by sediment dynamics and chemical properties (Fig. 11).

PAHs, which are largely associated with the particulate phase, show enhanced offshore dispersal following the flood event, with elevated concentrations in prodelta areas influenced by riverine plumes (Figs. 7 and ~~12~~11). This apparent offshore redistribution does not imply increased chemical mobility, but rather reflects the efficient transport of PAH-bearing fine particles during flood-driven sediment dispersal. This redistribution is consistent with the deposition of fine-grained, organic-rich sediments characterized by $\delta^{13}C$ signatures indicative of a predominantly terrigenous origin (Tesi et al., 2007; Bao et al., 2016; Broder et al., 2018; Hage et al., 2022; Nogarotto et al., 2023). These sediments act as efficient carriers for hydrophobic organic contaminants, including PAHs.

The grain-size dependence of PAH distribution and their strong positive correlation with TOC likely reflect the preferential sorption of PAHs onto natural organic matter (Hedges and Keil, 1999; Bucheli et al., 2004; Lohmann et al., 2005; Stout and Emsbo-Mattingly, 2008; Ukalska-Jaruga et al., 2018). The close correspondence between PAH concentrations and TOC has been widely documented in both marine and terrestrial sediments (Soclo et al., 2000; Rockne et al., 2002; Talley et al., 2002; Nascimento et al., 2017; Vane et al., 2007, 2020).

Consistently, PAH concentrations display a strong positive correlation with fine sediment fractions (clay and silt), while sand content is negatively correlated. This relationship may arise from PAHs being partitioned onto organic matter coatings associated with clay and silt particles and/or through direct adsorption onto clay mineral surfaces. In this context, organic matter behaves hydrodynamically similarly to the fine-grained fraction, facilitating the coupled transport and deposition of PAHs with clay-rich sediments during flood-driven dispersal. This suggests that hydrophobic organic contaminants follow the transport dynamics of organic-rich riverine clays, similar to other prodelta systems (Roussiez et al., 2006; Bouloubassi et al., 2012).

During flood events, the rapid delivery of fine-grained, organic-rich material enhances the efficiency of PAH transport by coupling contaminant partitioning with hydrodynamic sorting. This process promotes the selective offshore focusing of PAHs at the prodelta where fine sediments and organic matter accumulate (Fig. ~~12~~11). Indeed the Adriatic prodelta deposits, especially near the Misa River, show PAH concentrations up to five times higher than nearshore samples, creating focused pollutant hotspots of significant environmental concern (Fig. 11). Moreover, the spatial distribution of PAHs is heterogeneous and shaped by both diffuse and point sources, with elevated concentrations near urban and industrial centers such as Fano, Senigallia, and Ancona. These areas are influenced by harbor activities, vehicular traffic, and maritime transport (Frapiccini et al., 2024). Even mountainous areas, typically less impacted by anthropogenic activity, present detectable PAH levels, likely linked to fossil fuel combustion for domestic heating during winter. This demonstrates that short-lived flood events can generate spatially concentrated contaminant accumulation with potentially disproportionate ecological relevance.

In contrast, PFASs show a distinct spatial pattern due to their chemical properties, showing limited offshore dispersion regardless of sediment grain size, reflecting the complexity of contaminant-sediment interactions influenced by granulometry and chemical affinities and with highest concentrations confined near river mouths (Fig. 9 and Fig. 11). This pattern highlights a key difference in transport mechanisms: PFASs, unlike traditional persistent organic pollutants (POPs), are not primarily governed by sorption to organic matter. Their surfactant-like properties and amphiphilic structure cause them to interact distinctively with saline environments through processes such as the salting-out effect, which reduces their solubility as salinity increases, limiting offshore transport (Pan & You, 2010; Jeon et al., 2011; Wang et al., 2013; Munoz et al., 2017; Newell et al., 2021; Steffen et al., 2021; Li et al., 2022; Yin et al., 2022; Hort et al., 2024). This is evident in the 2022 flood event, where PFAS distribution was influenced by mixing of freshwater flood plumes with marine waters, resulting in preferential accumulation near the coast (Fig. 11).

Deeper sediment layers deposited prior to the 2022 flood showed minimal PFAS concentrations, with trace amounts of 6:2FTS detected in northern transects (A, Metauro, B, Cesano), suggesting historical contamination potentially linked to earlier flood or storm events. Surface sediments associated with the 2022 flood revealed 6:2FTS as the dominant compound, followed by 8:2FTS, reflecting the influence of newer-generation PFASs used as alternatives to banned legacy compounds (Field & Seow, 2017). Traditional PFASs such as PFHxA, PFOA, and PFUnA were widespread, with peak concentrations offshore of the

Formattato: Interlinea: doppia

Misa River, confirming Senigallia as a primary hotspot. Elevated PFAS levels were also recorded in the Metauro River transect, likely due to upstream industrial activities such as non-stick cookware manufacturing. Higher copper concentrations in these sediments corroborate anthropogenic pressure, although values remained below regulatory limits (120 mg kg^{-1}). This area remains under active environmental monitoring by regional agencies (e.g., ARPAM).

In summary, the spatial and compositional variability of pollutants observed in this study underscores the importance of event-based monitoring strategies. While the 2022 flood had a broad hydrodynamic footprint, its contaminant impact was spatially selective, reinforcing pre-existing gradients rather than creating uniformly distributed pollution. PAHs were redistributed more broadly due to their particulate-bound nature, whereas PFASs remained concentrated near-source due to their solubility and surfactant behavior (Fig. 11). These findings highlight the complex interplay between sediment dynamics and contaminant chemistry in shaping pollutant distribution following extreme hydrological events, with important implications for coastal ecosystem management and resilience.

Finally, the preferential accumulation of flood-transported sediments and associated pollutants at the 10–15 m isobath creates distinct biogeochemical 'hotspots' or pollutant sinks within the prodelta environment. This spatial segregation highlights the need to focus monitoring and remediation efforts on these depositional zones, which play a crucial role in controlling contaminant cycling and storage in coastal systems (Pellegrini et al., 2023).

~~Understanding the origin and behavior of contaminants in marine sediment is crucial for evaluating environmental and human health risks, as well as for implementing effective coastal management strategies (e.g. Neff et al., 2005; Di Lorenzo et al., 2020; Pizzini et al., 2021; Pellegrini et al., 2023; Trincardi et al., 2023). In this study, the spatial heterogeneity of sediment bound contaminants, including Polycyclic Aromatic Hydrocarbons (PAHs) and Poly- and Perfluorinated Alkyl Substances (PFASs), reveals differential transport and depositional pathways shaped by sediment dynamics and chemical properties (Fig. 12). PAHs, largely particulate-bound, exhibit wider offshore dispersal following the flood event, with concentrations increasing in prodelta areas influenced by riverine plumes (Fig. 7 and Fig. 12). This redistribution is consistent with the deposition of fine-grained, organic-rich sediments that exhibit a distinct $\delta^{13}C$ signature indicative of terrigenous origin (Tesi et al., 2007; Bao et al., 2016; Broder et al., 2018; Hage et al., 2022; Nogarotto et al., 2023), and which act as carriers for hydrophobic organic contaminants. This suggests that hydrophobic organic contaminants follow the transport dynamics of~~

~~organic-rich riverine clays, similarly to what has been described for other prodelta systems (e.g. Roussiez et al., 2006; Bouloubassi et al., 2012). The Adriatic prodelta deposits, especially near the Misa River, show PAH concentrations up to five times higher than nearshore samples, creating focused pollutant hotspots of significant environmental concern (Fig. 12). Moreover, the spatial distribution of PAHs is heterogeneous and shaped by both diffuse and point sources, with elevated concentrations observed near urban and industrial centers such as Fano, Senigallia, and Ancona. These areas are influenced by harbor activities, vehicular traffic, and maritime transport (Frapiccini et al., 2024). Even mountainous areas, typically less impacted by anthropogenic activity, present detectable PAHs levels, likely linked to fossil fuel combustion for domestic heating during winter.~~

~~In contrast, PFASs demonstrate a distinct spatial pattern, with the highest concentrations confined near river mouths and rapidly decreasing offshore (Fig. 9 and Fig. 12). This pattern highlights a key difference in transport mechanisms: PFASs, unlike traditional persistent organic pollutants (POPs), are not primarily governed by sorption to organic matter. Their surfactant-like properties and amphiphilic structure cause them to interact distinctively with saline environments through processes such as the salting-out effect, which reduces their solubility as salinity increases, limiting offshore transport (Pan and You, 2010; Jeon et al., 2011; Wang et al., 2013; Munoz et al., 2017; Newell et al., 2021; Steffen et al., 2021; Li et al., 2022; Yin et al., 2022; Hort et al., 2024). This is evident in the 2022 flood event, where PFAS distribution was influenced by the mixing of freshwater flood plumes with marine waters, resulting in preferential accumulation near the coast. Deeper sediment layers, deposited prior to the 2022 flood, showed minimal PFAS concentrations, with trace amounts of 6:2FTS detected in northern transects (A, Metauro, B, Cesano), suggesting historical contamination potentially linked to earlier flood or storm events. Surface sediments associated with the 2022 flood revealed 6:2FTS as the dominant compound, followed by 8:2FTS, reflecting the influence of newer-generation PFASs used as alternatives to banned legacy compounds (Field & Seow, 2017). Traditional PFASs such as PFHxA, PFOA, and PFUnA were widespread, with peak concentrations offshore of the Misa River, confirming Senigallia as a primary hotspot. Elevated PFAS levels were also recorded in the Metauro River transect, likely due to upstream industrial activities such as non-stick cookware manufacturing. Higher copper concentrations in these sediments corroborate anthropogenic pressure, although values remained below regulatory limits (120 mg kg^{-1}). This area remains under active environmental monitoring by regional agencies (e.g., ARPAM).~~

Summarizing, the spatial and compositional variability of pollutants observed in this study underscores the importance of event-based monitoring strategies. While the 2022 flood had a broad hydrodynamic footprint, its contaminant impact was spatially selective, reinforcing pre-existing gradients rather than creating uniformly distributed pollution. PAHs were redistributed more broadly due to their particulate-bound nature, whereas PFASs remained concentrated in near-source areas due to their solubility and surfactant behavior (Fig. 12). These findings emphasize the complex interaction between sediment dynamics and contaminant chemistry in shaping pollutant distribution following extreme hydrological events, with important implications for the management and resilience of coastal ecosystems.

River flood deposits and their role in shaping spatial heterogeneity of bacterial communities

The analysis of benthic prokaryotic community composition confirmed that the impact of the September 2022 flood event was not only limited to the nearshore zone, with the impact in the prodelta area appeared to be evident in the most affected river (Fig. 12). Variations in substrate composition and grain size shaped both the diversity and structure of microbial assemblages, suggesting that ephemeral depositional events of limited geological significance may have major biological consequences. The lower diversity observed closer to the coast, characterized by higher pollution levels, represents a pattern reported in previous studies, including those conducted in the Adriatic Sea (Quero et al., 2015).

The pronounced differences in composition of benthic prokaryotic community along the coast-to-sea transects corroborate the hypothesis of a spatial structuring of sedimentary microbiomes in response to coastal and fluvial inputs. Coastal samples formed a distinct cluster, characterized by higher relative abundances of Thermoanaerobaculaceae and Woeseiaceae, which correlated with the sandy sediment fraction (Fig. 10B). This suggests that coastal microbial communities are closely coupled with sediment granulometry and physicochemical gradients driven by terrestrial inputs (Fagervold et al. 2014; Fazi et al., 2020; Hamamoto et al., 2024), in accordance to previous studies reporting Thermoanaerobaculaceae as ubiquitous in coastal (Fonseca et al., 2022, Giner_Lamia et al., 2024) and disturbed sediments (Ramljak et al., 2024), and Woeseiaceae as cosmopolitan taxon in coastal, organic carbon-rich environments (Hoffmann et al., 2020; Tolar et al., 2020).

Offshore benthic prokaryotic communities exhibited greater heterogeneity and formed two subclusters, reflecting variable levels of exposure to the flood plume and sediment deposition (Figs. 10 and 12). Offshore sediment assemblages in front of

~~the Misa and Esino rivers and C transect appeared more impacted by the flood, supported by their association with higher clay, TOC, and TN levels (Fig. 12). These sites represent major deposition zones, where fine-grained particles transported offshore during the flood settled (Cattaneo et al., 2003; Pellegrini et al., 2015), reshaping the benthic habitat (Fig. 12). Such sedimentation patterns are consistent with the hydrodynamics of the Adriatic Sea, which promotes offshore transport of suspended materials during high-flow events (Langone et al., 2016; Marini et al., 2016).~~

~~The high relative abundance of Flavobacteriaceae and Vicinamibacteria suggests functional shifts in microbial communities driven by changes in sediment composition and riverine input, as similarly observed in other coastal environments (Quero et al., 2015; Giner-Lamia et al., 2024). The presence of Flavobacteriaceae and other freshwater-indicator taxa (such as Comamonadaceae, Fluviicola ecc.) in the most impacted offshore samples further supports a direct link between river discharge and microbial community restructuring. Differentiation within offshore sediments likely reflects spatial variability in exposure to recent flood-derived deposition, consistent with previous studies highlighting the influence of riverine sedimentation on benthic microbial assemblages (Cibic et al., 2019, Massaccesi et al., 2025). Overall, the reshaping of benthic prokaryotic communities in response to flood-derived sedimentation underscores the need to assess whether such alterations may exert lasting ecological consequences, and whether thay ultimately affect the resilience of coastal marine ecosystems.~~

5.~~3~~ 3 ~~A broad flood generating spatially restricted pollutant hotspots~~

Flood-derived sedimentation as a driver of benthic microbial community structure

To explore potential patterns associated with the September 2022 flood, we analyzed samples along a coastal-to-offshore transect. This analysis ~~aims~~ was designed to identify spatial associations rather than infer direct causality between flood forcing and microbial community change. Overall, our integrated microbial, sedimentological, and geochemical ~~view~~approach revealed that the 2022 flood triggered a targeted yet meaningful reorganization of benthic communities. The observed increase in microbial diversity with increasing distance from shore ~~Alpha diversity indices (Shannon diversity, ASV richness; Fig. 10A) indicate increasing microbial diversity offshore.~~generally reflect~~ing~~ed the presence of finer sediments and lower physical disturbance along the transect (Fig. 11). Nearshore sites, with coarser sediments, elevated PAHs and PFASs, and stronger wave disturbance, exhibited significantly lower microbial diversity, consistent with other coastal systems where physical stress and

pollutant exposure was associated with reduced richness and functional complexity (Quero et al., 2015; Cibic et al., 2019). Offshore assemblages were more diverse and taxonomically heterogeneous, forming subclusters associated with fine-grained, TOC- and TN-enriched sediments typical of flood deposits. The spatial overlap of fine-grained flood deposits, localized contaminant hotspots (notably PAHs and PFASs), and distinct microbial communities underscores the tight coupling between sediment transport and biogeochemical functioning. Fine sediments act as vectors for hydrophobic contaminants, concentrating pollutants in depositional hotspots such as the prodelta at 10–15 m water depth, which serve as key pollutant sinks. These environments may thus favor microbial assemblages adapted to organic-rich and contaminated conditions, including freshwater-derived taxa indicative of recent riverine inputs (Fig. 11). Both microbial community structure and the analysis of biomarker taxa revealed ~~Non-metric Multidimensional Scaling (nMDS; Fig. 10B) reveals~~ distinct communityies associated with~~clusters separating~~ nearshore, prodelta, and offshore ~~assemblages~~stations, with ~~while LEfSe analysis (Fig. 10C) highlights~~ taxa driving these differences~~,~~ often being linked to riverine or marine sedimentary environments (Fig. 10C). ~~These patterns demonstrate how flood-driven sediment dynamics directly influence microbial community composition by delivering distinct sediment types and associated contaminants.~~

~~In the Marche region offshore, microbial community structure shows a strong spatial gradient shaped by sediment grain size, organic content, contaminant load, and selective deposition of flood-derived sediments (Figs. 10 and 12). Nearshore sites, with coarser sediments, elevated PAHs and PFASs, and stronger wave disturbance, exhibit significantly lower microbial diversity (Fig. 12), consistent with other coastal systems where physical stress and pollutant exposure reduce richness and functional complexity (Quero et al., 2015; Cibic et al., 2019). Offshore assemblages are more diverse and taxonomically heterogeneous, forming subclusters associated with fine-grained, TOC- and TN-enriched sediments typical of flood deposits (Figs. 4 and 10B).~~ The presence of freshwater-indicator taxa (Flavobacteriaceae, Vicinamibacteria, Comamonadaceae) supports the hypothesis of a direct riverine influence on offshore communities ~~(Supplementary Fig. S3)~~, aligning with previous findings on flood-driven dispersal (Giner-Lamia et al., 2024; Massaccesi et al., 2025). Moreover,

~~T~~the spatial confinement of these "flood-influenced" microbial signatures reflects physical sediment transport limits imposed by meteo-oceanographic conditions ~~(Fig. 12)~~. The northeasterly storm following the flood ~~(Fig. 11)~~ enhanced offshore transport of fine particles while restricting their dispersion beyond the 15 m isobath, shaping both sedimentary and biological

patterns (Fig. 11). Thus, hydrodynamic processes not only regulate sediment and contaminant dispersal, but it might also indirectly ~~constrain~~affect microbial community assembly~~s~~ages diversity and functioning (Voynova et al., 2017; Fazi et al., 2020; Steichen et al., 2020; Jajun et al., 2024; Vona et al., 2025) ~~. Importantly, the spatial overlap of fine-grained flood deposits, localized contaminant hotspots (notably PAHs and PFASs), and distinct microbial communities underscores the tight coupling between sediment transport and biogeochemical functioning. Fine sediments act as vectors for hydrophobic contaminants, concentrating pollutants in depositional hotspots such as the prodelta at 10–15 m water depth, which serve as key pollutant sinks. These environments favor microbial assemblages adapted to organic-rich and contaminated conditions, including freshwater-derived taxa indicative of recent riverine inputs.~~

Overall, our findings suggest that, ~~Such interactions suggest that,~~ despite the transient nature of flood sediment deposits, flood-driven sediment dynamics may directly shape benthic microbial communities by delivering~~f~~ distinct sediment types and associated contaminants, and that ecologically meaningful shifts in benthic ecosystem functioning can occur. Taken together, these spatially constrained patterns raise the broader ~~qeustion~~question of how increasingly frequent or intense flood events may translate into persistent, long-term changes in coastal ecosystems.

Although limited, available post-flood studies consistently indicate that repeated flood-driven inputs alter coastal carbon and nutrient budgets as well as oxygen dynamics over seasonal to multiannual timescales (Sommerfield and Nittrouer, 1999; Geyer et al., 2000; Drexler and Nittrouer, 2005; Tesi et al., 2013; Steichen et al., 2020). The magnitude, direction and possible recovery of these biological and biogeochemical shifts in response to recurrent exposure to such perturbations ~~Recent research further suggests that flood events reshape microbial assembly mechanisms by weakening environmental filtering, enhancing dispersal, and intensifying biotic interactions, thereby modifying community structure, keystone taxa, and network stability (Voynova et al., 2017; Fazi et al., 2020; Steichen et al., 2020; Jajun et al., 2024; Vona et al., 2025). Together, these findings support the notion that the apparent ephemerality of individual flood events does not preclude longer-term ecological consequences. Instead, cumulative hydrological forcing associated with increasingly frequent floods may progressively shape coastal microbial assemblages and ecosystem functioning.~~ emphasiz~~ics~~ng the need for integrated, long-term~~.~~ event-focused monitoring coupling microbial and geochemical data, particularly ~~. Moreover, floods act as vectors for anthropogenic pollutants and pathogens, imposing persistent selective pressures on coastal microbial communities (Smith and Casadevall~~

2022; Yu, 2025). Recurrent exposure to such perturbations may thus progressively influence sedimentary biogeochemistry, contaminant retention, and microbially mediated processes. These considerations highlight the critical importance of long-term perspectives in regions prone to frequent extreme hydrological events.

Overall, this integrated microbial, sedimentological, and geochemical view reveals that the 2022 flood triggered a targeted yet meaningful reorganization of benthic communities. While the sedimentary imprint was ephemeral, the cumulative impact of repeated high-magnitude floods on prodelta geochemistry, contaminant accumulation, and microbial communities, over decadal scales, can drive significant shifts in biogeochemical cycling and ecosystem structure. Overall, these insights underscore the critical importance of rapid-response surveys, which are essential to capture short-lived sedimentary and ecological signals that would otherwise remain undetected by conventional monitoring approaches.

Changes in microbial community structure likely cascade into sediment biogeochemistry, modulating carbon mineralization, nitrogen transformations, contaminant degradation, sediment oxygen demand, and nutrient fluxes, all critical to coastal ecosystem functioning. However, the magnitude and direction of these biogeochemical shifts remain uncertain without long-term, integrated monitoring coupling microbial and geochemical data. Understanding ecosystem resilience and recovery amid increasing flood frequency thus requires multidisciplinary, time-resolved studies.

The benthic microbial community structure exhibits a clear spatial gradient shaped by sediment grain size, organic matter content, contaminant load, and the selective deposition of flood-derived sediments (Figs. 10 and 12). Nearshore stations, characterized by coarser textures, elevated PAH and PFAS concentrations, and stronger wave-induced disturbance, hosted significantly lower microbial diversity (Fig. 12). This pattern aligns with observations from other deltaic and coastal systems, where physical stress and pollutant exposure reduce richness and functional complexity (Quero et al., 2015; Cibic et al., 2019). In contrast, offshore assemblages were markedly more diverse and taxonomically heterogeneous, forming consistent subclusters associated with fine-grained, TOC-TN-enriched sediments typical of flood deposits (Figs. 4 and 10B). The presence of freshwater-indicator taxa, including Flavobacteriaceae, Vicinamibacteria, and Comamonadaceae, further supports the direct influence of riverine inputs on offshore microbial communities (Supplementary Fig. S3). These taxa have been

~~reported as markers of freshwater and flood-driven dispersal in previous studies (Massaccesi et al., 2025; Giner-Lamia et al., 2024).~~

~~The spatial confinement of these "flood-influenced" microbial signatures mirrors the physical limits of sediment transport imposed by meteo-oceanographic conditions (Fig. 12). The northeasterly storm following the flood (Fig. 11) enhanced the offshore transport of fine particles while simultaneously restricting their dispersion beyond the 15 m isobath, thus shaping not only the sedimentary record but also the biological imprint. This coupling between sediment advection and microbial community restructuring highlights how short-lived hydrodynamic events can produce lasting ecological effects despite leaving subtle stratigraphic traces.~~

~~Overall, the integration of microbial, sedimentological, and geochemical data indicates that the 2022 flood induced a targeted but ecologically significant reorganization of benthic communities. These changes illustrate how episodic sedimentation events modulate benthic ecosystem functions and resilience, emphasizing the need for multidisciplinary approaches to interpret the full impact of extreme hydrological disturbances in coastal systems.~~

CONCLUSIONS

The September 2022 flood produced a spatially discontinuous and short-lived sedimentary signal ~~in the offshore zone~~at sea, strongly controlled by sediment grain size and coastal meteo-oceanographic dynamics. Fluvial inputs were largely confined to the prodelta, where reduced wave-induced shear stress allowed for the temporary deposition of fine-grained sediments. In contrast, sandy nearshore zones experienced intense wave and current-driven resuspension and alongshore transport, limiting sediment accumulation and preservation. Strong Bora-driven hydrodynamics further inhibited offshore sediment dispersion beyond the 15 m isobath, resulting in patchy sediment layers with limited preservation potential. This transient sedimentary imprint poses challenges for the recognition and stratigraphic archiving of extreme flood deposits in marine settings.

Flood-induced sediment heterogeneity also shaped benthic microbial assemblages. In coarse, sandy coastal sediments, microbial communities exhibited lower diversity and were characterized by taxa such as Thermoanaerobaculaceae and Woeseiaceae, likely reflecting increased physical disturbance and contaminant exposure. Conversely, fine-grained, organic-

rich prodelta deposits supported diverse prokaryotic communities, including freshwater-derived taxa indicative of recent riverine input. These findings highlight how even ephemeral sedimentary events can produce spatially structured microbial ecosystem responses, with important implications for benthic functioning and biogeochemical cycling.

Regarding pollutants, the analysis of PAHs and PFASs revealed that marine sediment contamination results from a complex interplay between chronic anthropogenic pressures and episodic events. The 2022 flood facilitated the redistribution of both traditional and emerging contaminants, with the Misa River and adjacent coastal areas identified as hotspots of concern. PAHs, largely bound to fine organic particles, exhibited wider offshore dispersal following the flood, while PFASs, influenced by their chemical properties, remained concentrated near river mouths. These patterns emphasize the need for targeted monitoring and remediation strategies, especially in flood-prone, industrialized coastal regions where contaminant dynamics and concentrations are highly event-dependent.

Although the 2022 flood left an ephemeral sedimentary signal, the cumulative impact of repeated high-magnitude flood events on prodelta geochemistry, contaminant inventories, and benthic microbial communities depends on the variable preservation of individual deposits. Dynamic coastal processes such as wave-induced resuspension and subsequent flood events can partially or entirely rework earlier flood deposits, leading to a non-linear and intermittent stratigraphic record. Nonetheless, over decadal timescales, this cumulative influence may drive significant shifts in coastal biogeochemical cycling and ecosystem structure.

Overall, this study underscores the value of multidisciplinary approaches in understanding coastal responses to extreme hydrological events. By integrating sediment transport, hydrodynamics, microbial ecology, and contaminant behavior, we achieve a more comprehensive understanding of how floods affect the land–sea interface. Recognizing the ephemeral yet impactful nature of such events is essential not only for interpreting recent sedimentary records but also for anticipating future environmental consequences in the Mediterranean and other climatically sensitive coastal systems.

ACKNOWLEDGMENTS

This project has received funding from the Italian Ministry of Research under the PRIN ON-OFF project contract 2022PMEN2K, and by EU - Next Generation EU Mission 4, Component 2 - CUP B53C22002150006 - Project IR0000032 – ITINERIS - Italian Integrated Environmental Research Infrastructures System. The Authors want to thank Silvio Davolio (CNR-ISAC), Pierluigi Penna (CNR-IRBIM) e Silvia Unguendoli (ARPAE) for respectively MOLOCH, TeleSenigallia, and ADRIAC data provision. Federico Falcini is thanked for sharing orthophoto images.

REFERENCES

Adeoba, M. I., Pandelani, T., Ngwangwa, H., & Masebe, T. (2025). The Role of Artificial Intelligence in Sustainable Ocean Waste Tracking and Management: A Bibliometric Analysis. Sustainability, 17(9), 3912.

Ainsworth, R. B., Vakarelov, B. K., & Nanson, R. A. (2011). Dynamic spatial and temporal prediction of changes in depositional processes on clastic shorelines: toward improved subsurface uncertainty reduction and management. *AAPG bulletin*, *95*(2), 267-297.

Allan, R. P., & Soden, B. J. (2008). Atmospheric warming and the amplification of precipitation extremes. Science, 321(5895), 1481-1484. Anthony, E., Syvitski, J., Zăinescu, F., Nicholls, R. J.,

Amorosi, A., & Sammartino, I. (2007). Influence of sediment provenance on background values of potentially toxic metals from near-surface sediments of Po coastal plain (Italy). *International journal of earth sciences*, *96*(2), 389-396.

Amorosi, A., Guermandi, M., Marchi, N., & Sammartino, I. (2014). Fingerprinting sedimentary and soil units by their natural metal contents: a new approach to assess metal contamination. *Science of the Total Environment*, *500*, 361-372.

Amorosi, A., Sammartino, I., Dinelli, E., Campo, B., Guercia, T., Trincardi, F., & Pellegrini, C. (2022). Provenance and sediment dispersal in the Po-Adriatic source-to-sink system unraveled by bulk-sediment geochemistry and its linkage to catchment geology. *Earth-Science Reviews*, *234*, 104202.

Anthony, E. J., Marriner, N., & Morhange, C. (2014). Human influence and the changing geomorphology of Mediterranean deltas and coasts over the last 6000 years: From progradation to destruction phase?. *Earth-Science Reviews*, *139*, 336-361.

Anthony, E., Syvitski, J., Zăinescu, F., Nicholls, R. J., Cohen, K. M., Marriner, N., ... & Maselli, V. (2024). Delta sustainability from the Holocene to the Anthropocene and envisioning the future. *Nature Sustainability*, *7*(10), 1235-1246.

Arienzo, M., Donadio, C., Mangoni, O., Bolinesi, F., Stanislao, C., Trifuoggi, M., Toscanesi, M., Di Natale, G., Ferrara, L., 2017. Characterization and source apportionment of polycyclic aromatic hydrocarbons (pahs) in the sediments of gulf of Pozzuoli (Campania, Italy). Marine pollution bulletin 124, 480-487. http://dx.doi.org/10.1016/j.marpolbul.2017.07.006

Bao, R., McIntyre, C., Zhao, M., Zhu, C., Kao, S. J., & Eglinton, T. I. (2016). Widespread dispersal and aging of organic carbon in shallow marginal seas. *Geology*, *44*(10), 791-794.

Bao, R., van der Voort, T. S., Zhao, M., Guo, X., Montluçon, D. B., McIntyre, C., & Eglinton, T. I. (2018). Influence of hydrodynamic processes on the fate of sedimentary organic matter on continental margins. *Global Biogeochemical Cycles*, *32*(9), 1420-1432.

Basili, M., Campanelli, A., Frapiccini, E., Luna, G. M., & Quero, G. M. (2021). Occurrence and distribution of microbial pollutants in coastal areas of the Adriatic Sea influenced by river discharge. *Environmental Pollution*, *285*, 117672.

Baumard, P.; Budzinski, H.; Garrigues, P. Polycyclic aromatic hydrocarbons in sediments and mussels of the western Mediterranean Sea. Environ. Toxicol. Chem. Int. J. 1998, 17, 765–776.

Benincasa, M., Falcini, F., Adduce, C., Sannino, G., & Santoleri, R. (2019). Synergy of satellite remote sensing and numerical ocean modelling for coastal geomorphology diagnosis. Remote Sensing, 11(22), 2636.

Bentley, S. J., & Nittrouer, C. A. (2003). Emplacement, modification, and preservation of event strata on a flood-dominated continental shelf: Eel shelf, Northern California. *Continental Shelf Research*, *23*(16), 1465-1493.

ha formattato: Inglese (Stati Uniti)

ha formattato: Colore carattere: Nero, Inglese (Stati Uniti)

Codice campo modificato

ha formattato: Tipo di carattere: Colore carattere: Nero, Inglese (Regno Unito)

Bhattacharya, J. P., & MacEachern, J. A. (2009). Hyperpycnal rivers and prodeltaic shelves in the Cretaceous seaway of North America. *Journal of Sedimentary Research*, *79*(4), 184-209.

Bianchi, T. S., Morrison, E., Barry, S., Arellano, A. R., Feagin, R. A., Hinson, A., ... & Oviedo-Vargas, D. (2018). The fate and transport of allochthonous blue carbon in divergent coastal systems. In *A blue carbon primer* (pp. 27-49). CRC Press.

Bisci, G. Cantalamessa, G.M. Luna, E. Manini, E. Frapiccini, F. Spagnoli, M. Tramontana, G. Scalella, S. Parlani, M. Sinigaglia, G. Forchielli, F. Mazzoli, D. Magnoni, C. Bellino, D. Pernini., 2021. Qualità dei sedimenti di retro scogliera nelle Marche. Studi costieri 2021 - 29: 29 – 28

Blöschl, G., Hall, J., Parajka, J., Perdigão, R. A., Merz, B., Arheimer, B., ... & Živković, N. (2017). Changing climate shifts timing of European floods. *Science*, *357*(6351), 588-590.

Blott, S. J., & Pye, K. (2001). GRADISTAT: a grain size distribution and statistics package for the analysis of unconsolidated sediments. *Earth surface processes and Landforms*, *26*(11), 1237-1248.

Blum, M. D., & Roberts, H. H. (2009). Drowning of the Mississippi Delta due to insufficient sediment supply and global sea-level rise. *Nature geoscience*, *2*(7), 488-491.

Bolan, L.P. Padhye, T. Jasemizad, M. Govarthanan, N. Karmegam, H. Wijesekara, D. Amarasiri, D. Hou, P. Zhou, B.K. Biswal, R. Balasubramanian, H. Wang, K.H.M. Siddique, J. Rinklebe, M.B. Kirkham, N. Bolan, 2024. Impacts of climate change on the fate of contaminants through extreme weather events, Science of The Total Environment, 909, 168388, https://doi.org/10.1016/j.scitotenv.2023.168388.

Book, J. W., R. P. Signell, and H. Perkins (2007), Measurements of storm and nonstorm circulation in the northern Adriatic: October 2002 through April 2003, *J. Geophys. Res.*, 112, C11S92, doi:10.1029/2006JC003556.

Bosman, A., Romagnoli, C., Madricardo, F., Correggiari, A., Remia, A., Zubalich, R., ... & Trincardi, F. (2020). Short-term evolution of Po della Pila delta lobe from time lapse high-resolution multibeam bathymetry (2013–2016). *Estuarine, Coastal and Shelf Science*, *233*, 106533.

Bouloubassi, I., Roussiez, V., Azzoug, M., & Lorre, A. (2012). Sources, dispersal pathways and mass budget of sedimentary polycyclic aromatic hydrocarbons (PAH) in the NW Mediterranean margin, Gulf of Lions. *Marine Chemistry*, *142*, 18-28.

Bue, G. L., Musa, M., Marchini, A., Riccardi, M. P., Dubois, S. F., Lisco, S., ... & Mancin, N. (2025). Microplastic pollution in the littoral environment: insights from the largest Mediterranean Sabellaria spinulosa (Annelida) reef and shoreface sediments. *Marine Pollution Bulletin*, *217*, 118132.

Bressan, L., Valentini, A., Paccagnella, T., Montani, A., Marsigli, C., and Tesini, M. S.: Sensitivity of sea-level forecasting to the horizontal resolution and sea surface forcing for different configurations of an oceanographic model of the Adriatic Sea, Adv. Sci. Res., 14, 77–84, https://doi.org/10.5194/asr-14-77-2017, 2017.

Callahan, B. J., McMurdie, P. J., Rosen, M. J., Han, A. W., Johnson, A. J. A., & Holmes, S. P. (2016). DADA2: High-resolution sample inference from Illumina amplicon data. *Nature methods*, *13*(7), 581-583.

Campanelli, A., Grilli, F., Paschini, E., & Marini, M. (2011). The influence of an exceptional Po River flood on the physical and chemical oceanographic properties of the Adriatic Sea. *Dynamics of Atmospheres and Oceans*, *52*(1-2), 284-297.

Cattaneo, A., Trincardi, F., Asioli, A., & Correggiari, A. (2007). The Western Adriatic shelf clinoform: energy-limited bottomset. *Continental Shelf Research*, *27*(3-4), 506-525.

ha formattato: Tedesco (Germania)

Codice campo modificato

ha formattato: Inglese (Stati Uniti)

Cibic, T., Fazi, S., Nasi, F., Pin, L., Alvisi, F., Berto, D., & Del Negro, P. (2019). Natural and anthropogenic disturbances shape benthic phototrophic and heterotrophic microbial communities in the Po River Delta system. *Estuarine, Coastal and Shelf Science*, *222*, 168-182.

Coleman, J. M., & Wright, L. D. (1975). Modern river deltas: variability of processes and sand bodies. Houston Geological Society, 99-149.

Cohen, K. M., Marriner, N., & Maselli, V. (2024). Delta sustainability from the Holocene to the Anthropocene and envisioning the future. Nature Sustainability, 7(10), 1235-1246.
Gardner, J., Pavelsky, T., Topp, S., Yang, X., Ross, M. R., & Cohen, S. (2023). Human activities change suspended sediment concentration along rivers. Environmental Research Letters, 18(6), 064032.

Cohen, S., Syvitski, J., Ashley, T., Lammers, R., Fekete, B., & Li, H. Y. (2022). Spatial trends and drivers of bedload and suspended sediment fluxes in global rivers. Water resources research, 58(6), e2021WR031583.

Davolio S, Henin R, Stocchi P, Buzzi A. 2017. Bora wind and heavy persistent precipitation: atmospheric water balance and role of air-sea fluxes over the Adriatic Sea. Q J R Meteorol Soc. 143(703):1165–1177.

De Lucia, C., Amaddii, M., & Arrighi, C. (2024). Tangible and intangible ex post assessment of flood-induced damage to cultural heritage. *Natural Hazards and Earth System Sciences*, *24*(12), 4317-4339.

T. Di Lorenzo, G.C. Hose, D.M.P. Galassi, Assessment of different contaminants in freshwater: origin, fate and ecological impact. Water 12(6), 1810 (2020). https://doi.org/10.3390/w12061810

Dinelli, E., Lucchini, F., Fabbri, M., & Cortecci, G. (2001). Metal distribution and environmental problems related to sulfide oxidation in the Libiola copper mine area (Ligurian Apennines, Italy). *Journal of Geochemical Exploration*, *74*(1-3), 141-152.

Dinelli, E., Lucchini, F., Mordenti, A., & Paganelli, L. (1999). Geochemistry of Oligocene–Miocene sandstones of the northern Apennines (Italy) and evolution of chemical features in relation to provenance changes. *Sedimentary Geology*, *127*(3-4), 193-207.

Donnini, M., Santangelo, M., Gariano, S. L., Bucci, F., Peruccacci, S., Alvioli, M., ... & Fiorucci, F. (2023). Landslides triggered by an extraordinary rainfall event in Central Italy on September 15, 2022. *Landslides*, *20*(10), 2199-2211.

Dottori, F., Mentaschi, L., Bianchi, A., Alfieri, L., & Feyen, L. (2023). Cost-effective adaptation strategies to rising river flood risk in Europe. *Nature Climate Change*, *13*(2), 196-202.

Fagervold, S. K., Bourgeois, S., Pruski, A. M., Charles, F., Kerherve, P., Vetion, G., & Galand, P. E. (2014). River organic matter shapes microbial communities in the sediment of the Rhône prodelta. *The ISME journal*, *8*(11), 2327-2338.

Fain, A. M. V., Ogston, A. S., & Sternberg, R. W. (2007). Sediment transport event analysis on the western Adriatic continental shelf. *Continental Shelf Research*, *27*(3-4), 431-451.

Falcini, F., Khan, N. S., Macelloni, L., Horton, B. P., Lutken, C. B., McKee, K. L., ... & Jerolmack, D. J. (2012). Linking the historic 2011 Mississippi River flood to coastal wetland sedimentation. *Nature Geoscience*, *5*(11), 803-807.

~~M. Fanelli, S. Illuminati, A. Annibaldi, R. De Marco, C. Cerotti, F. Girolametti, B. Ajdini, C. Truzzi, E. Frapiccini, A. Gallerani, M. Tramontana, G. Baldelli, F. Spagnoli, 2025. Mercury historical signature in the Central and Southern Adriatic Sea sediment cores, Estuarine, Coastal and Shelf Science, 314, 109144, https://doi.org/10.1016/j.ecss.2025.109144.~~

Fanelli, M., Illuminati, S., Annibaldi, A., De Marco, R., Cerotti, C., Girolametti, F., ... & Spagnoli, F. (2025). Mercury historical signature in the Central and Southern Adriatic Sea sediment cores. *Estuarine, Coastal and Shelf Science*, *314*, 109144.

Fazi, S., Baldassarre, L., Cassin, D., Quero, G. M., Pizzetti, I., Cibic, T., ... & Del Negro, P. (2020). Prokaryotic community composition and distribution in coastal sediments following a Po river flood event (northern Adriatic Sea, Italy). *Estuarine, Coastal and Shelf Science*, *233*, 106547.

Field, J. A., & Seow, J. (2017). Properties, occurrence, and fate of fluorotelomer sulfonates. *Critical Reviews in Environmental Science and Technology*, *47*(8), 643-691.

Fonseca, A., Espinoza, C., Nielsen, L. P., Marshall, I. P., & Gallardo, V. A. (2022). Bacterial community of sediments under the eastern boundary current system shows high microdiversity and a latitudinal spatial pattern. *Frontiers in Microbiology*, *13*, 1016418.

Fowler, H. J., Lenderink, G., Prein, A. F., Westra, S., Allan, R. P., Ban, N., ... & Zhang, X. (2021). Anthropogenic intensification of short-duration rainfall extremes. *Nature Reviews Earth & Environment*, *2*(2), 107-122.

Franzini, M., Leoni, L., & Saitta, M. (1972). A simple method to evaluate the matrix effects in X-Ray fluorescence analysis. *X-ray Spectrometry*, *1*(4), 151-154.

Franzini, M., Leoni, L., & Saitta, M. (1975). *Revisione di una metodologia analitica per fluorescenza-X, basata sulla correzione completa degli effetti di matrice.* Rendiconti della Società Italiana di Mineralogia e Petrologia, 31, 365–378

E. Frapiccini, R. De Marco, F. Grilli, M. Marini, A. Annibaldi, E. Prezioso, M. Tramontana, F. Spagnoli, 2024. Anthropogenic contribution, transport, and accumulation of Polycyclic Aromatic Hydrocarbons in sediments of the continental shelf and slope in the Mediterranean Sea, Chemosphere, 352, 141285. https://doi.org/10.1016/j.chemosphere.2024.141285

Friedrichs, C. T., & Scully, M. E. (2007). Modeling deposition by wave-supported gravity flows on the Po River prodelta: from seasonal floods to prograding clinoforms. *Continental Shelf Research*, *27*(3-4), 322-337.

Gardner, J., Pavelsky, T., Topp, S., Yang, X., Ross, M. R., & Cohen, S. (2023). Human activities change suspended sediment concentration along rivers. *Environmental Research Letters*, *18*(6), 064032.

Giner-Lamia, J., & Huerta-Cepas, J. (2024). Exploring the sediment-associated microbiota of the Mar Menor coastal lagoon. *Frontiers in Marine Science*, *11*, 1319961.

Goodbred Jr, S. L. (2003). Response of the Ganges dispersal system to climate change: a source-to-sink view since the last interstade. *Sedimentary Geology*, *162*(1-2), 83-104.

Gomez, B., Mertes, L. A., Phillips, J. D., Magilligan, F. J., & James, L. A. (1995). Sediment characteristics of an extreme flood: 1993 upper Mississippi River valley. *Geology*, *23*(11), 963-966.

Govindaraju, K. (1989). 1989 compilation of working values and sample description for 272 geostandards. *Geostandards Newsletter*, *13*, 1-113.

Gruca-Rokosz, R., Cieśla, M., Kida, M., & Ignatowicz, K. (2025). Spatio-Temporal Patterns of Polycyclic Aromatic Hydrocarbons and Phthalates Deposition in Sediments of Reservoirs: Impact of Some Environmental Factors. *Water*, *17*(5), 641.

Gupta, D., Hazarika, B. B., Berlin, M., Sharma, U. M., & Mishra, K. (2021). Artificial intelligence for suspended sediment load prediction: a review. *Environmental earth sciences*, *80*(9), 346.

ha formattato: Inglese (Stati Uniti)

ha formattato: Inglese (Stati Uniti)

Hamamoto, K., Mizuyama, M., Nishijima, M., Maeda, A., Gibu, K., Poliseno, A., ... & Reimer, J. D. (2024). Diversity, composition and potential roles of sedimentary microbial communities in different coastal substrates around subtropical Okinawa Island, Japan. *Environmental Microbiome*, *19*(1), 54.

Haq, B., & Milliman, J. (2023). Perilous future for river deltas. *GSA Today*, *33*(10), 4-12.

Harris, C. K., Sherwood, C. R., Signell, R. P., Bever, A. J., & Warner, J. C. (2008). Sediment dispersal in the northwestern Adriatic Sea. *Journal of Geophysical Research: Oceans*, *113*(C11).

Hoffmann, K., Bienhold, C., Buttigieg, P. L., Knittel, K., Laso-Pérez, R., Rapp, J. Z., ... & Offre, P. (2020). Diversity and metabolism of Woeseiales bacteria, global members of marine sediment communities. *The ISME journal*, *14*(4), 1042-1056.

Hood, W. G. (2010). Tidal channel meander formation by depositional rather than erosional processes: examples from the prograding Skagit River Delta (Washington, USA). *Earth Surface Processes and Landforms: The Journal of the British Geomorphological Research Group*, *35*(3), 319-330.

Hort, H. M., Robinson, C. E., Sawyer, A. H., Li, Y., Cardoso, R., Lee, S. A., ... & Newell, C. J. (2024). Conceptualizing controlling factors for PFAS salting out in groundwater discharge zones along sandy beaches. *Groundwater*, *62*(6), 860-875.

IPCC, 2021, Climate Change 2021: The Physical Science Basis. Contribution of Working Group I to the Sixth Assessment Report of the Intergovernmental Panel on Climate Change: Cambridge, UK, and New York, Cambridge University Press, 2391 p., https://doi.org/10.1017/9781009157896.

Jaramillo, S., Sheremet, A., Allison, M. A., Reed, A. H., & Holland, K. T. (2009). Wave-mud interactions over the muddy Atchafalaya subaqueous clinoform, Louisiana, United States: Wave-supported sediment transport. *Journal of Geophysical Research: Oceans*, *114*(C4).

Jeon, J., Kannan, K., Lim, B. J., An, K. G., & Kim, S. D. (2011). Effects of salinity and organic matter on the partitioning of perfluoroalkyl acid (PFAs) to clay particles. Journal of Environmental Monitoring, 13(6), 1803-1810.

Jolaosho, T. L., Rasaq, M. F., Omotoye, E. V., Araomo, O. V., Adekoya, O. S., Abolaji, O. Y., & Hungbo, J. J. (2025). Microplastics in freshwater and marine ecosystems: Occurrence, characterization, sources, distribution dynamics, fate, transport processes, potential mitigation strategies, and policy interventions. Ecotoxicology and Environmental Safety, 294, 118036.

Korus, J. T., & Fielding, C. R. (2015). Asymmetry in Holocene river deltas: patterns, controls, and stratigraphic effects. *Earth-Science Reviews*, *150*, 219-242.

Kundzewicz, Z. W., Kanae, S., Seneviratne, S. I., Handmer, J., Nicholls, N., Peduzzi, P., ... & Sherstyukov, B. (2014). Flood risk and climate change: global and regional perspectives. *Hydrological Sciences Journal*, *59*(1), 1-28.

Kundzewicz, Z. W., Pińskwar, I., & Brakenridge, G. R. (2018). Changes in river flood hazard in Europe: a review. Hydrology research, 49(2), 294-302.

Langone, L., et al. Dynamics of particles along the western margin of the Southern Adriatic: Processes involved in transferring particulate matter to the deep basin. *Marine Geology*, 2016, 375: 28-43

Leoni, L., & Saitta, M. (1976). Determination of yttrium and niobium on standard silicate rocks by X-ray fluorescence analyses. *X-ray Spectrometry*, *5*(1), 29-30.

ha formattato: Inglese (Stati Uniti)

Leoni, L., Menichini, M., & Saitta, M. (1982). Determination of S, Cl and F in silicate rocks by X-Ray fluorescence analyses. X-Ray Spectrometry, 11(4), 156-158.

Li, C., Zhang, C., Gibbes, B., Wang, T., & Lockington, D. (2022). Coupling effects of tide and salting-out on perfluorooctane sulfonate (PFOS) transport and adsorption in a coastal aquifer. Advances in Water Resources, 166, 104240.

Liu, J. P., Li, A. C., Xu, K. H., Velozzi, D. M., Yang, Z. S., Milliman, J. D., & DeMaster, D. J. (2006). Sedimentary features of the Yangtze River-derived along-shelf clinoform deposit in the East China Sea. *Continental Shelf Research*, *26*(17-18), 2141-2156.

Lee, C.C., Chen, C.S., Wang, Z.X., Tien, C.J., 2021. Polycyclic aromatic hydrocarbons in 30 river ecosystems, Taiwan: sources, and ecological and human health risks. Sci. Total Environ. 795, 1–14. https://doi.org/10.1016/j.scitotenv.2021.148867.

Lehmann, J., Coumou, D., & Frieler, K. (2015). Increased record-breaking precipitation events under global warming. *Climatic Change*, *132*, 501-515.

Lim, K. Y., Zakaria, N. A., & Foo, K. Y. (2021). Geochemistry pollution status and ecotoxicological risk assessment of heavy metals in the Pahang River sediment after the high magnitude of flood event. Hydrology Research, 52(1), 107-124.

Lohrenz, S. E., Dagg, M. J., & Whitledge, T. E. (1990). Enhanced primary production at the plume/oceanic interface of the Mississippi River. *Continental shelf research*, *10*(7), 639-664.

Lucchini F., Frignani M., Sammartino I., Dinelli E., Bellucci L.G. (2001). Composition of Venice Lagoon sediments: distribution, sources, settings and recent evolution. GeoActa 1, 7-20.

Macquaker, J. H., Bentley, S. J., & Bohacs, K. M. (2010). Wave-enhanced sediment-gravity flows and mud dispersal across continental shelves: Reappraising sediment transport processes operating in ancient mudstone successions. *Geology*, *38*(10), 947-950.

Maletíc, S.P., Beljin, J.M., Roñcevíc, S.D., Grgíc, M.G., Dalmacija, B.D., 2019. State of the art and future challenges for polycyclic aromatic hydrocarbons is sediments: sources, fate, bioavailability and remediation techniques. J. Hazard Mater. 365, 467–482. https://doi.org/10.1016/j.jhazmat.2018.11.020.

Mali, M., Ragone, R., Dell'Anna, M.M., Romanazzi, G., Damiani, L., Mastrorilli, P., 2022. Improved identification of pollution source attribution by using PAH ratios combined with multivariate statistics. Sci. Rep. 12, 1–13. https://doi.org/10.1038/s41598-022-23966-4.

Marini, M., Maselli, V., Campanelli, A., Foglini, F., & Grilli, F. (2016). Role of the Mid-Adriatic deep in dense water interception and modification. *Marine Geology*, *375*, 5-14.

Martin, M. (2011). Cutadapt removes adapter sequences from high-throughput sequencing reads. *EMBnet. journal*, *17*(1), 10-12.

Massaccesi, N., Basili, M., Coci, M., Cassin, D., Zonta, R., Manini, E., ... & Quero, G. M. (2025). Benthic prokaryotic diversity in Po River Delta lagoons (North Adriatic Sea) is shaped by riverine freshwater inputs. *Estuarine, Coastal and Shelf Science*, 109348.

Mayer, L. M. (1994). Surface area control of organic carbon accumulation in continental shelf sediments. *Geochimica et Cosmochimica Acta*, *58*(4), 1271-1284.

McMurdie, P. J., & Holmes, S. (2013). phyloseq: an R package for reproducible interactive analysis and graphics of microbiome census data. *PloS one*, *8*(4), e61217.

ha formattato: Inglese (Stati Uniti)

Codice campo modificato

Mead, R. N., & Goñi, M. A. (2008). Matrix protected organic matter in a river dominated margin: A possible mechanism to sequester terrestrial organic matter?. *Geochimica et Cosmochimica Acta*, *72*(11), 2673-2686.

Merz, B., Blöschl, G., Vorogushyn, S., Dottori, F., Aerts, J. C., Bates, P., ... & Macdonald, E. (2021). Causes, impacts and patterns of disastrous river floods. *Nature Reviews Earth & Environment*, *2*(9), 592-609.

Milliman, J. D., & Syvitski, J. P. (1992). Geomorphic/tectonic control of sediment discharge to the ocean: the importance of small mountainous rivers. The journal of Geology, 100(5), 525-544.

MSFD, 2008. Directive 2008/56/EC of the European Parliament and of the Council stablishing a framework for community action in the field of marine environmental policy (Marine Strategy Framework Directive). OJ L 164, 25.6.2008, p. 19–40.

Munoz, G., Budzinski, H., & Labadie, P. (2017). Influence of environmental factors on the fate of legacy and emerging per- and polyfluoroalkyl substances along the salinity/turbidity gradient of a macrotidal estuary. Environmental science & technology, 51(21), 12347-12357.

Neff, J.M., Stout, S.A., Gunster, D.G., 2005. Ecological risk assessment of polycyclic aromatic hydrocarbons in sediments: identifying sources and ecological hazard. Integr Environ Asses 1, 22–23. https://doi.org/10.1897/IEAM_2004a-016.1.

Nie, J., Sobel, A. H., Shaevitz, D. A., & Wang, S. (2018). Dynamic amplification of extreme precipitation sensitivity. Proceedings of the National Academy of Sciences, 115(38), 9467-9472.

Nikki, R., Jaleel, K. A., Razaque, M. A., Gupta, P., Rathore, C., Saha, M., ... & Kumar, T. G. (2025). Assessment of hazardous microplastic polymers and phthalic acid esters in an invasive mollusk (Mytella strigata) from the Cochin estuary, southwest coast of India: Unraveling ecosystem risks. Science of The Total Environment, 967, 178798.

Nittrouer, C. A., Kuehl, S. A., DeMaster, D. J., & Kowsmann, R. O. (1986). The deltaic nature of Amazon shelf sedimentation. *Geological Society of America Bulletin*, *97*(4), 444-458.

Oksanen, J., Simpson, G. L., Blanchet, F. G., Kindt, R., Legendre, P., Minchin, P. R., ... & Weedon, J. (2001). Vegan: community ecology package. *(No Title)*.

Overeem, I., & Brakenridge, R. G. (Eds.). (2009). *Dynamics and vulnerability of delta systems* (Vol. 35). GKSS Research Centre, LOICZ Internat. Project Office, Inst. for Coastal Research.

Owowenu, E. K., Nnadozie, C. F., Akamagwuna, F., Siwe-Noundou, X., & Odume, O. N. (2025). Occurrence and distribution of microplastics in functionally delineated hydraulic zones in selected Rivers, Eastern Cape, South Africa. *Environmental Pollution*, 126544.

Palinkas, C. M., & Nittrouer, C. A. (2006). Clinoform sedimentation along the Apennine shelf, Adriatic Sea. *Marine Geology*, *234*(1-4), 245-260.

Palinkas, C. M., & Nittrouer, C. A. (2007). Modern sediment accumulation on the Po shelf, Adriatic Sea. *Continental Shelf Research*, *27*(3-4), 489-505.

Pan, G., & You, C. (2010). Sediment–water distribution of perfluorooctane sulfonate (PFOS) in Yangtze River Estuary. Environmental pollution, 158(5), 1363-1367.

Parada, A.E., Needham, D.M. and Fuhrman, J.A., 2016. Every base matters: assessing small subunit rRNA primers for marine microbiomes with mock communities, time series and global field samples. Environmental microbiology, 18(5), pp.1403-1414.

Codice campo modificato

ha formattato: Olandese (Paesi Bassi)

ha formattato: Inglese (Stati Uniti)

ha formattato: Inglese (Stati Uniti)

Patruno, S., & Helland-Hansen, W. (2018). Clinoforms and clinoform systems: Review and dynamic classification scheme for shorelines, subaqueous deltas, shelf edges and continental margins. *Earth-Science Reviews*, *185*, 202-233.

Peng, Y., Yu, Q., Du, Z., Wang, L., Wang, Y., & Gao, S. (2022). Gravity-driven sediment flows on the shallow sea floor of a muddy open coast. *Marine Geology*, *445*, 106759.

Pellegrini, C., Sammartino, I., Schieber, J., Tesi, T., Paladini de Mendoza, F., Rossi, V., & Amorosi, A. (2024). On depositional processes governing along-strike facies variations of fine-grained deposits: Unlocking the Little Ice Age subaqueous clinothems on the Adriatic shelf. *Sedimentology*, *71*(3), 941-973.

Pellegrini, C., Saliu, F., Bosman, A., Sammartino, I., Raguso, C., Mercorella, A., & Rovere, M. (2023). Hotspots of microplastic accumulation at the land-sea transition and their spatial heterogeneity: The Po River prodelta (Adriatic Sea). *Science of The Total Environment*, *895*, 164908.

Pellegrini, C., Tesi, T., Schieber, J., Bohacs, K. M., Rovere, M., Asioli, A., & Trincardi, F. (2021). Fate of terrigenous organic carbon in muddy clinothems on continental shelves revealed by stratal geometries: Insight from the Adriatic sedimentary archive. *Global and Planetary Change*, *203*, 103539.

Pellegrini, C., Patruno, S., Helland-Hansen, W., Steel, R. J., & Trincardi, F. (2020). Clinoforms and clinothems: Fundamental elements of basin infill. Basin Research, 32(Clinoforms and Clinothems: Fundamental Elements of Basin Infill), 187-205.

Pellegrini, C., Maselli, V., Cattaneo, A., Piva, A., Ceregato, A., & Trincardi, F. (2015). Anatomy of a compound delta from the post-glacial transgressive record in the Adriatic Sea. *Marine Geology*, *362*, 43-59.

Pierdomenico, M., Ridente, D., Casalbore, D., Di Bella, L., Milli, S., & Chiocci, F. L. (2022). Plastic burial by flash-flood deposits in a prodelta environment (Gulf of Patti, Southern Tyrrhenian Sea). Marine Pollution Bulletin, 181, 113819.

Pitarch, J., Falcini, F., Nardin, W., Brando, V. E., Di Cicco, A., & Marullo, S. (2019). Linking flow-stream variability to grain size distribution of suspended sediment from a satellite-based analysis of the Tiber River plume (Tyrrhenian Sea). Scientific reports, 9(1), 19729.

Pizzini, S., Giubilato, E., Morabito, E., Barbaro, E., Bonetto, A., Calgaro, L., ... & Marcomini, A. (2024). Contaminants of emerging concern in water and sediment of the Venice Lagoon, Italy. *Environmental Research*, *249*, 118401.

Pizzini, S., Morabito, E., Gregoris, E., Vecchiato, M., Corami, F., Piazza, R., & Gambaro, A. (2021). Occurrence and source apportionment of organic pollutants in deep sediment cores of the Venice Lagoon. *Marine Pollution Bulletin*, *164*, 112053.

Pomaro, A., Cavaleri, L. & Lionello, P. Climatology and trends of the Adriatic Sea wind waves: analysis of a 37-year long instrumental data set. *International Journal of Climatology* **37**(12), 4237–4250 (2017).

Poulain, P. M. (2001). Adriatic Sea surface circulation as derived from drifter data between 1990 and 1999. *Journal of Marine Systems*, *29*(1-4), 3-32.

Puig, P., Ogston, A. S., Guillén, J., Fain, A. M. V., & Palanques, A. (2007). Sediment transport processes from the topset to the foreset of a crenulated clinoform (Adriatic Sea). *Continental Shelf Research*, *27*(3-4), 452-474.

Pulvirenti, L., Squicciarino, G., Fiori, E., Candela, L., & Puca, S. (2023). Analysis and processing of the COSMO-SkyMed second generation images of the 2022 marche (Central Italy) flood. *Water*, *15*(7), 1353.

Quero, G. M., Cassin, D., Botter, M., Perini, L., & Luna, G. M. (2015). Patterns of benthic bacterial diversity in coastal areas contaminated by heavy metals, polycyclic aromatic hydrocarbons (PAHs) and polychlorinated biphenyls (PCBs). *Frontiers in microbiology*, *6*, 1053.

Ramljak, A., Žučko, J., Lučić, M., Babić, I., Morić, Z., Fafanđel, M., ... & Petrić, I. (2024). Microbial communities as indicators of marine ecosystem health: Insights from coastal sediments in the eastern Adriatic Sea. *Marine pollution bulletin*, *205*, 116649.

Ranjbar Jafarabadi, A., Riyahi Bakhtiari, A., Shadmehri Toosi, A., 2017. Comprehensive and comparative ecotoxicological and human risk assessment of polycyclic aromatic hydrocarbons (PAHs) in reef surface sediments and coastal seawaters of Iranian Coral Islands, Persian Gulf. Ecotoxicol. Environ. Saf. 145, 640–652. https://doi.org/ 10.1016/j.ecoenv.2017.08.016.

Rath, P., Panda, U. C., Bhatta, D., & Sahu, K. C. (2009). Use of sequential leaching, mineralogy, morphology and multivariate statistical technique for quantifying metal pollution in highly polluted aquatic sediments—A case study: Brahmani and Nandira Rivers, India. *Journal of Hazardous materials*, *163*(2-3), 632-644.

Ravaioli, M., Bergami, C., Riminucci, F., Langone, L., Cardin, V., Di Sarra, A., & Crise, A. (2016). The RITMARE Italian Fixed-Point Observatory Network (IFON) for marine environmental monitoring: a case study. Journal of Operational Oceanography, 9(sup1), s202-s214.
Regione Marche. (2016). Studio sulle analisi ambientali in aria (aggiornato a giugno 2019). Dipartimento di Ingegneria Industriale e Scienze Matematiche, Università Politecnica delle Marche. Ultima consultazione Regione Marche il 20/06/2024.

Riminucci, F., Funari, V., Ravaioli, M., & Capotondi, L. (2022). Trace metals accumulation on modern sediments from Po river prodelta, North Adriatic Sea. *Marine Pollution Bulletin*, *175*, 113399.

Roussiez, V., Ludwig, W., Monaco, A., Probst, J. L., Bouloubassi, I., Buscail, R., & Saragoni, G. (2006). Sources and sinks of sediment-bound contaminants in the Gulf of Lions (NW Mediterranean Sea): a multi-tracer approach. *Continental Shelf Research*, *26*(16), 1843-1857.

Sammartino, I. (2004). Heavy-metal anomalies and bioavailability from soils of southeastern Po Plain. *GeoActa*, *3*, 35-42.

Sanchez-Vidal, A., Higueras, M., Martí, E., Liquete, C., Calafat, A., Kerhervé, P., & Canals, M. (2013). Riverine transport of terrestrial organic matter to the North Catalan margin, NW Mediterranean Sea. *Progress in oceanography*, *118*, 71-80.

Schieber, J. (2013). SEM observations on ion-milled samples of Devonian black shales from Indiana and New York: the petrographic context of multiple pore types.

Schimmelmann, A., Riese, D. J., & Schieber, J. (2015, March). Fast and economical sampling and resin-embedding technique for small cores of unconsolidated, fine-grained sediment. In *Proceedings of the 2015 Pacific Climate (PACLIM) Workshop, Asilomar Conference Grounds, Pacific Grove, CA, USA* (pp. 8-11).

Sherwood, C. R., Book, J. W., & Harris, C. K. (2015). Sediment dynamics in the Adriatic Sea investigated with coupled models. *Oceanography*, *17*(4), 58.

Signell, R. P., Chiggiato, J., Horstmann, J., Doyle, J. D., Pullen, J., & Askari, F. (2010). High-resolution mapping of Bora winds in the northern Adriatic Sea using synthetic aperture radar. *Journal of Geophysical Research: Oceans*, *115*(C4).

Simon-Sánchez, L., Grelaud, M., Garcia-Orellana, J., & Ziveri, P. (2019). River Deltas as hotspots of microplastic accumulation: The case study of the Ebro River (NW Mediterranean). *Science of the total environment*, *687*, 1186-1196.

Slater, L., Villarini, G., Archfield, S., Faulkner, D., Lamb, R., Khouakhi, A., & Yin, J. (2021). Global changes in 20-year, 50-year, and 100-year river floods. *Geophysical Research Letters*, *48*(6), e2020GL091824.

Steffens, S. D., Cook, E. K., Sedlak, D. L., & Alvarez-Cohen, L. (2021). Under-reporting potential of perfluorooctanesulfonic acid (PFOS) under high-ionic strength conditions. Environmental Science & Technology Letters, 8(12), 1032-1037.

ha formattato: Francese (Francia)

ha formattato: Tedesco (Germania)

Sun, Q., Zhang, X., Zwiers, F., Westra, S., & Alexander, L. V. (2021). A global, continental, and regional analysis of changes in extreme precipitation. *Journal of Climate*, *34*(1), 243-258.

Syvitski, J., Ángel, J. R., Saito, Y., Overeem, I., Vörösmarty, C. J., Wang, H., & Olago, D. (2022). Earth's sediment cycle during the Anthropocene. Nature Reviews Earth & Environment, 3(3), 179-196.

Syvitski, J. P., & Kettner, A. J. (2007). On the flux of water and sediment into the Northern Adriatic Sea. *Continental Shelf Research*, *27*(3-4), 296-308.

Syvitski, J. P., Kettner, A. J., Overeem, I., Hutton, E. W., Hannon, M. T., Brakenridge, G. R., ... & Nicholls, R. J. (2009). Sinking deltas due to human activities. *Nature Geoscience*, *2*(10), 681-686.

Syvitski, J. P., Peckham, S. D., Hilberman, R., & Mulder, T. (2003). Predicting the terrestrial flux of sediment to the global ocean: a planetary perspective. Sedimentary Geology, 162(1-2), 5-24.

Syvitski, J. P., Vörösmarty, C. J., Kettner, A. J., & Green, P. (2005). Impact of humans on the flux of terrestrial sediment to the global coastal ocean. *science*, *308*(5720), 376-380.

Tesi, T., Langone, L., Giani, M., Ravaioli, M., & Miserocchi, S. (2013). Source, diagenesis, and fluxes of particulate organic carbon along the western Adriatic Sea (Mediterranean Sea). *Marine Geology*, *337*, 156-170.

Tesi, T., Miserocchi, S., Goni, M. E. A., Langone, L., Boldrin, A., & Turchetto, M. (2007). Organic matter origin and distribution in suspended particulate materials and surficial sediments from the western Adriatic Sea (Italy). *Estuarine, Coastal and Shelf Science*, *73*(3-4), 431-446.

Tesi, T., Miserocchi, S., Langone, L., Boni, L., & Guerrini, F. (2006). Sources, fate and distribution of organic matter on the western Adriatic continental shelf, Italy. *Water, Air, & Soil Pollution: Focus*, *6*(5), 593-603.

Tolar, B. B., Boye, K., Bobb, C., Maher, K., Bargar, J. R., & Francis, C. A. (2020). Stability of floodplain subsurface microbial communities through seasonal hydrological and geochemical cycles. *Frontiers in Earth Science*, *8*, 338.

Traykovski, P., Geyer, W. R., Irish, J. D., & Lynch, J. F. (2000). The role of wave-induced density-driven fluid mud flows for cross-shelf transport on the Eel River continental shelf. *Continental shelf research*, *20*(16), 2113-2140.

Traykovski, P., Wiberg, P. L., & Geyer, W. R. (2007). Observations and modeling of wave-supported sediment gravity flows on the Po prodelta and comparison to prior observations from the Eel shelf. *Continental Shelf Research*, *27*(3-4), 375-399.

Trincardi, F., Amorosi, A., Bosman, A., Correggiari, A., Madricardo, F., & Pellegrini, C. (2020). Ephemeral rollover points and clinothem evolution in the modern Po Delta based on repeated bathymetric surveys. *Basin Research*, *32*(Clinoforms and Clinothems: Fundamental Elements of Basin Infill), 402-418.

Trincardi, F., Francocci, F., Pellegrini, C., d'Alcalà, M. R., & Sprovieri, M. (2023). The Mediterranean Sea in the Anthropocene. In Oceanography of the Mediterranean Sea (pp. 501-553). Elsevier.

Vona, I., Colella, S., Sammartino, M., Brando, V. E., & Falcini, F. (2025). Positive correlation between the Po River discharge and ocean colour trends of Chl and TSM in the Adriatic Sea. Frontiers in Remote Sensing, 6, 1574347.

Vörösmarty, C. J., Meybeck, M., Fekete, B., Sharma, K., Green, P., & Syvitski, J. P. (2003). Anthropogenic sediment retention: major global impact from registered river impoundments. Global and planetary change, 39(1-2), 169-190.

ha formattato: Tedesco (Germania)

ha formattato: Tedesco (Germania)

Wang, X. H., & Pinardi, N. (2002). Modeling the dynamics of sediment transport and resuspension in the northern Adriatic Sea. *Journal of Geophysical Research: Oceans*, *107*(C12), 18-1.

Wang, S., Wang, H., & Deng, W. (2013). Perfluorooctane sulfonate (PFOS) distribution and effect factors in the water and sediment of the Yellow River Estuary, China. Environmental monitoring and assessment, 185(10), 8517-8524.

Warner J C, Armstrong B, He R and Zambon J B (2010) Development of a coupled ocean–atmosphere–wave–sediment transport (COAWST) modeling system Ocean Model. 35 230–44

Warrick, J. A., Buscombe, D., Vos, K., Bryan, K. R., Castelle, B., Cooper, J. A. G., ... & Young, A. P. (2024). Coastal shoreline change assessments at global scales. Nature communications, 15(1), 2316.

Weiss, L., Estournel, C., Marsaleix, P., Mikolajczak, G., Constant, M., & Ludwig, W. (2024). From source to sink: part 1—characterization and Lagrangian tracking of riverine microplastics in the Mediterranean Basin. *Environmental Science and Pollution Research*, 1-24.

Wentworth, C. K. (1922). A scale of grade and class terms for clastic sediments. *The journal of geology*, *30*(5), 377-392.

Westra, S., Alexander, L. V., & Zwiers, F. W. (2013). Global increasing trends in annual maximum daily precipitation. *Journal of climate*, *26*(11), 3904-3918.

Wheatcroft, R. A. (2000). Oceanic flood sedimentation: a new perspective. *Continental Shelf Research*, *20*(16), 2059-2066.

Wheatcroft, R. A., & Drake, D. E. (2003). Post-depositional alteration and preservation of sedimentary event layers on continental margins, I. The role of episodic sedimentation. *Marine Geology*, *199*(1-2), 123-137.

Wheatcroft, R. A., Goñi, M. A., Hatten, J. A., Pasternack, G. B., & Warrick, J. A. (2010). The role of effective discharge in the ocean delivery of particulate organic carbon by small, mountainous river systems. *Limnology and Oceanography*, *55*(1), 161-171.

Winsemius, H. C., Aerts, J. C., Van Beek, L. P., Bierkens, M. F., Bouwman, A., Jongman, B., ... & Ward, P. J. (2016). Global drivers of future river flood risk. Nature Climate Change, 6(4), 381-385.

Yin, C., Pan, C. G., Xiao, S. K., Wu, Q., Tan, H. M., & Yu, K. (2022). Insights into the effects of salinity on the sorption and desorption of legacy and emerging per-and polyfluoroalkyl substances (PFASs) on marine sediments. Environmental Pollution, 300, 118957.

Yunker, M.B., Macdonald, R.W., Vingarzan, R., Mitchell, R.H., Goyette, D., Sylvestre, S., 2002. PAHs in the Fraser River basin: a critical appraisal of PAH ratios as indicators of PAH source and composition. Organic Geochemistry 33, 489-515.

ha formattato: Inglese (Stati Uniti)

ha formattato: Inglese (Stati Uniti)

ha formattato: Olandese (Paesi Bassi)